Analysis and visualization of multivariate causality and information flow between event related conditions on Field Dependent – Field Independent EEG data

by

AIKATERINI LYMPERIDOU

BSc. in Mathematics, University of Crete

A THESIS

Submitted in partial fulfillment of the requirements for the degree

MASTER OF SCIENCE

INTERDISCIPLINARY GRADUATE PROGRAMME IN THE BRAIN AND MIND SCIENCES

SCHOOL OF MEDICINE

UNIVERSITY OF CRETE

Examination Committee:

Vangelis Sakkalis

Adonis Moschovakis

Stelios Smirnakis

Heraklion, Crete

2020

Examination Committee:

Vangelis Sakkalis (Supervisor)

Computational BioMedicine Lab (CBML)

Institute of Computer Science (ICS), Foundation for Research and Technology (FORTH), Heraklion

Email: sakkalis@ics.forth.gr

Adonis K. Moschovakis (Advisor)

Professor of Physiology, Faculty of Medicine, University of Crete

Computational Neuroscience group, IACM, Foundation for Research and Technology (FORTH), Heraklion

Email: moschova@uoc.gr

Stelios M. Smirnakis (Advisor)

Department of Neurology, Brigham and Women's Hospital, Jamaica Plain VA Hospital

Associate Professor of Neurology, Harvard Medical School, Boston

Email: smsmirnakis@bwh.harvard.edu

Submitted in partial fulfillment of the requirements for the degree Master of Science,
INTERDISCIPLINARY GRADUATE PROGRAMME IN THE BRAIN AND MIND SCIENCES,
School of Medicine, University of Crete
In the Computation BioMedicine Lab, Institute of Computer Science (ICS), Foundation for Research and Technology (FORTH), Heraklion

Contents

1. Introduction

Cognition is the mental process of acquiring knowledge and understanding, through memory, judgement and decision-making[1]. Cognitive learning style describes how the learner approaches learning through all the above intellectual functions. It is about the manner of obtaining the knowledge (Miron, Erez, & Naveh, 2004). The field dependence/independence are two cognitive style dimensions based on the individual's ability to extract particular meaning from the context (Ehrman & Leaver, 2003). This relatively stable pattern of information processing (Dillon & Watson, 1996)is one of the most broadly studied in the literature. These dimensions describe two different ways to acquire, organize and interpret information: Field Dependent (FD) and Field Independent (FI) learners. In general, FI learners are motivated by competition, individual recognition and analytical activities that do not necessitate a group type approach. FD learners prefer to work with others to achieve a common goal and they like to learn by experimentation (Ariza, 2002). Furthermore, there are significant differences between these groups in memory, cognition, compensation and social strategy use (Naraghipour & Baghestani, n.d.).

Differences between the FDI groups in terms of search tasks and eye gaze patterns have also been subject for studies(E. A. Nisiforou & Laghos, 2013; E. Nisiforou & Laghos, 2016). In this study, we will focus on the main difference between the FD and FI groups in visual perception: the ability of extracting a cue from a complex figure. The FI group is better in the discrimination of objects in a background, while the FD group is less able to identify a cue without its surroundings (Zhang, 2004). We will study this difference with the use of an experiment that takes on ambiguous images. These reversible or ambiguous figures are images which exploit graphical similarities to interpret two distinct image forms although the visual stimulus is stable and does not change. Rubin's vase (Parkkonen, Andersson, Hämäläinen, & Hari, 2008) and My Wife and My Mother in Law (published by William Ely Hill in an American humor magazine on 1915) are two classic examples of ambiguous images. A perceptual reversal is reported between the mental states corresponding to the two interpretations of the image.

FIGURE 1 EXAMPLES OF AMBIGUOUS IMAGES: RUBIN'S VASE, MY WIFE AND MY MOTHER IN LAW

[1] Definition of cognition in English from the Oxford dictionary, www.oxforddictionaries.com. Retrieved 2016-02-04

Due to its high temporal resolution compared to other techniques (MRI, PET, CT) Encephalography (EEG) is the ideal method to study the brain activity of the FDI groups. EEG is an electrophysiological method to record the difference in the electric potential resulting from ionic current within the neurons of the brain. The electrodes are sensors that convert the ion current inside the human head to current of electrons. The contact between the electrode and the skin is achieved with the help of a special gel that plays the role of an electrolyte. When there is electrical activity inside the brain, there is a difference in the electric potential between the two layers and as a result, there is electron flow in the electrode. The places that we set the electrodes on the head depends on the prototype International System 10-20 (Kannathal, Choo, Acharya, & Sadasivan, 2005). In our task we used the electrodes FP1, F7, FC1, C3, T7, CP1, CP5, TP9, P3 and O1 on the left hemisphere and the FP2, F8, FC2, C4, T8, CP2, CP6, TP10, P4, O2 on the right hemisphere. Also, Fz, Cz and Cpz were the center electrodes. Each of the above electrode denotes its position from its name. The letter shows the area of the head that the electrode is placed (i.e. F-Frontal, O-Occipital). Even numbers correspond to electrodes on the right hemisphere and the odd correspond to the left hemisphere. An extra third electrode, called ground electrode, is needed for getting differential voltage by subtracting the same voltages showing at active and reference points.

The electrical human EEG signal is about 10 μV to 100 μV in amplitude when measured from the scalp. As a result, an amplifier is needed to strengthen the signal and dense coverage from the electrodes to capture the low electrical activity. The EEG signal has different waveforms based on the frequency of their harmonics called rhythms. The basic brain rhythms are Alpha, Beta, Gamma, Theta and Delta.

Delta band appears during sleep. Theta rhythm reflects drowsiness and inhibition in elicited responses. Alpha rhythm appears in adults during the closure of the eyes and relaxation periods. Beta rhythm is correlated with high alertness and active thinking. Gamma band is associated with cross-modal sensory processing and short term memory recognized objects.

The EEG signal is related with the brain activities and the level of arousal of the person. High brain activation results in high frequencies and short amplitude on the waveforms. For example, when the human eyes are closed, we notice mainly the alpha rhythm (8-13 Hz). In addition, we could detect pathologies like epilepsy or schizophrenia and abnormal brain states during sleep etc. With this thesis, we are interested to know in which frequency band we could notice differences between the FDI groups on a visual perception and on a discrimination of figures task. More specifically, there are two main purposes in this research: (a) to figure out some Granger causality connectivity features that could significantly differentiate FD from FI group and in which frequency bands, (b) to confirm if there are findings indicating a perceptual reversal in our experiment.

We applied Multivariate Autoregression (MVAR) Modeling (Chapter 3.1) in the EEG channels and created a graph for each subject showing the interaction between the main brain Regions of Interest (ROIs). We estimate the interaction flow through the Directed Transfer Function (DTF) (Chapter 4.1), a function based on the Granger causality concept (Chapter 3.2). We calculate specific connectivity measures (Chapter 4.2) to quantify the differences between the two FDI groups. In particular, the methodology was:

- Preprocessing of the data (Chapter 5.2),
- Clustering for identifying the Regions of Interest (ROI) (Chapter 5.3),

- Source localization for calculating the EEG signal source in each ROI (Chapter 5.4),
- Estimation of the brain connectivity (Chapter 6.1) and
- Statistical results of our connectivity measures (Chapter 6.2).

2. Field dependent and Field Independent group

Two theories have dominated about the phenomenon of reversal of ambiguous figures. The first theory (bottom-up), the satiation, has a sensory adaptation approach and called the fatiguing of the neural process responsible for one perception that leads to the suspension of that process: when that happens the process responsible for the alternative perception occurs. The second theory (top-down), the cognitive approach suggests that reversal is a process of intention and learning. The fact that the subjects know that a figure is ambiguous and also know the two perceptions of the image leads them to engage in some form of motivated mental activity pressing for reversal(Rock, Hall, & Davis, 1994). Some researchers denote that both processes are combined for the achievement of the perceptual reverse(Intaite, Koivisto, Rukšenas, & Revonsuo, 2010).

A lot of studies, focus on the brain areas responsible for the bistable perception(M. Wang, Arteaga, & He, 2013; X. Wang et al., 2017; Weilnhammer, Stuke, Hesselmann, Sterzer, & Schmack, 2017). The EEG due to its high temporal resolution captures the brain activity at the precise time of the reversal event (V. Sakkalis, 2011). The best way to distinguish the exact timing of the reversal in the signal analysis is the manual response that we used in our research, where subjects indicate the time of the reversal by pressing a button (Kornmeier & Bach, 2012). The experimental set up in the majority of the studies, based on the same ambiguous figure as the Boring's young/old woman (Boring, 1930; Kornmeier & Bach, 2014)and the Necker cube (Kornmeier & Bach, 2005; Mathes, Strüber, Stadler, & Basar-Eroglu, 2006). However, in this study we used different random stimulis (ambiguous images) to figure out if the perceptual reversal could still be detected even if there is no intention of seeing the same ambiguous image in every trial.

Occipital areas get involved in the visual perception task, but also temporal and parietal locations constitute areas that show high activation too.(Kornmeier & Bach, 2014)suggests that more and different types of stimuli involves other areas of process of the ambiguity, like Fusiform Face Area (FFA), except the occipital areas. The perceptual reversal indicates a change in the perceived spatial structure of the figure and as a result transforms the participant's viewpoint in the 3D space. Parietal and temporal areas are involved in the neural processes that underlie in human spatial abilities. Temporal and parahimppocampal cortices are involved in topographic memory and navigation while the parietal lobe is responsible for spatial perception and representation of extrapersonal space (A. D. Ekstrom, 2010)(Colby, 2001). (Goode, Goddard, & Pascual-Leone, 2002) suggested that the larger amplitudes in FD participants reflects the inhibition process they must mobilize in order to change their usual global passive perception.

The research depending on the perceptual reversal focus on the event-related potentials (ERPs) and frequency related features. In the time window 128-154 ms after the

onset of the experiment and in the 274-292 ms there is a reversal negativity. Furthermore, a late positivity exhibited in the frontal and parietal areas during 423-471 ms(Britz, Landis, & Michel, 2009).

About the frequency related features, a slow reduction is detected 1000 ms before the button press denoting the endogenous reversal (Strüber & Herrmann, 2002). Another study investigated the frequency bands of an ambiguity task and revealed an increase in gamma band in frontal locations during the same period of time (1000 ms) before the manual response (Başar-Eroglu, Strüber, Kruse, Başar, & Stadler, 1996). Also a decrease in the alpha power observed in the P300-like component (reversal positivity) about 250 ms before the reversal button press (Isoglu-Alkaç et al., 2000)

There are not a lot of studies about brain connectivity using time series analysis and MVAR process during an ambiguity task. (Maksimenko et al., 2019)used a connectivity measure called recurrence-based measure of dependence (RMD) that determines the presence of a causal relation in a pair of processes. This analysis revealed a large scale functional network in the beta frequency band with the pronounced driving role of frontal cortical areas. Motivated by the fact that not a lot of studies conducted with the estimation of the brain connectivity, we decided to explore the characteristics of the FDI groups through the MVAR process and the measure based on the Granger causality principle, the DTF function.

3. EEG Parametric modeling

The human nervous system consists from plenty of neural networks that operate with an interactive way with each other (L. Lee, Harrison, & Mechelli, 2003). Effective connectivity may be defined as the direct or the indirect influence that one neural system exerts over another. The research on the brain effective connectivity contribute to understand better the functions of the brain. The main research approach based on the information coded on the frequency spectrum of the EEG signal. Techniques of signal processing based on frequency estimate metrics that highlight interdependency between the signals: correlation coefficient (Matousek, 1973), the coherence (Lachaux et al., 2002), generalized phase synchronization (D. S. Lee, Kye, Rim, Kwon, & Kim, 2003).

Brain connectivity could be calculate from brain activity time series from Electroencephalography, Local Field Potentials or spike trains and are separated in two categories: the bivariate and the multivariate estimators. In the framework of multivariate autoregressive model we define a basic measure based on the Granger causality principle: Directed Transfer Function (Kaminski & Blinowska, 1991).

Beside the research based on the relation between the different regions of the brain, another approach is to explore if there is any causality between them. Granger Causality (GC) is the relationship resulting between two time series whether the first time series is useful in forecasting the second one (Eichler, 2012; Granger, 1980). Specifically, the time series X it is said to Granger cause another time series Y if predictions of the value of Y based on its own past values and on the past values of X help to linearly predict future values of process Y beyond what can be achieved by using past values of process Y alone. Causality has been used to explore the effective connectivity (directed information flow, or causality) in the brain based on event-related relationships between channel waveforms.

To explore the causality between brain areas, we need to define the directionality and the intensity of their interaction. With the use of the bivariate autoregressive modeling we achieve to verge these metrics, but only for the correlation between two signals and without taking into account the influence of all the other structures of the system (Pereda, Quiroga, & Bhattacharya, 2005). This sometimes leads to misleading results (Kuś, Kamiński, & Blinowska, 2004).

To overcome these restrictions, the multivariate modeling has been proposed as a more precise estimation of the interaction between the multichannel signals. The MVAR modeling is one of the most common methods to explore the spectrum characteristics of the signals because it is an understandable, easy to solve and provide accurate estimation of the power spectrum density.

3.1 MVAR modeling

The multivariate autoregressive (MVAR) model describes for each time series the linear contribution coming from its past samples and the past samples of all other time series(Hytti, Takalo, & Ihalainen, 2006). The MVAR model is strictly causal due to the modeling only of the lagged effects and not of the instantaneous effects. Any zero-lag correlation among time series is translated like a correlation among the model residuals (Korhonen et al., 1996).

The set of M zero-mean time series $X(n) = \chi_1(n), \chi_2(n), \dots, \chi_M(n)$is described by the MVAR model

$$X(n) = \sum_{k=1}^{p} A(k)X(n-k) + U(n) \qquad (Eq.1)$$

Where p is the model order, $A(k)$ are the $M \times M$ matrices containing the elements $A_{ij}(k)$, namely the model coefficients, that describe the linear interaction at lag k from $\chi_j(n-k)$ to $\chi_i(n)(i,j = 1, \dots, M)$ and $U(n) = [u_1(n), \dots, u_M(n)]^T$ is a vector of zero mean white noise process. As referred above any zero-lag cross correlations are explained by correlations among the input noises$U$.

Below we can see a schematic of sliding window MVAR modeling that show exactly the procedure of transforming the EEG signals to adjacency matrices[2].

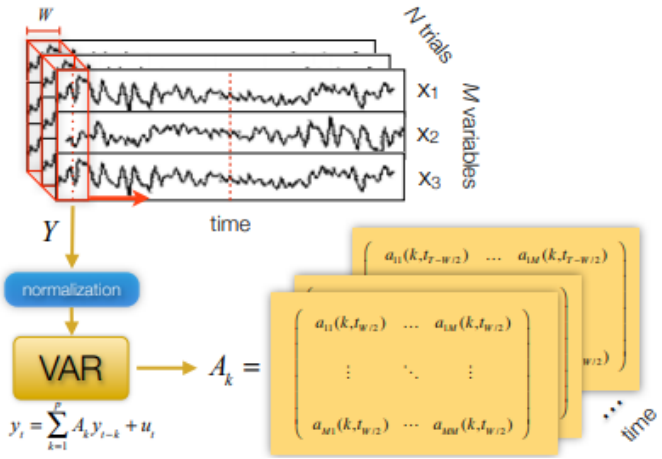

FIGURE 2 SCHEMATIC OF SLIDING WINDOW MVAR MODELING

[2] Source: SIFT manual (https://sccn.ucsd.edu/wiki/SIFT)

In terms of Granger causality the MVAR model could be described as a procedure that χ_i causes χ_j if the fact that we know the past states of χ_i (i.e. $\chi_j\,(n-1), \chi_j\,(n-2)$ … $\chi_j\,(n-k)$) guides to a better prediction of χ_j. In terms of mathematics, χ_i causesχ_j if at least one off diagonal element $A_{ij}\,(k)$ of the matrices A is significantly different from zero (Erla, Faes, Tranquillini, Orrico, & Nollo, 2009).

Two basic conditions, stationarity and stability must be satisfied regarding the data X and its MVAR model. We should notice at this point that stability implies stationarity, so it is sufficient to test for stability to ensure that a VAR process satisfies both of these criteria. Evoked or event related data appear to violate these assumptions, so adaptive or time varying methods have been developed to relax stationarity assumptions (Kitajo, Hanakawa, Ilmoniemi, & Miniussi, 2015)(Ding, Bressler, Yang, & Liang, 2000).
Thus, a stochastic process X is weakly stationary (or wide sense stationary) if its mean and covariance do not change in time.

$$\mathrm{E[X]} = \mu\,, \qquad Cov(X_t, Y_s) = r(t-s)$$

Where μ is a constant and r is an appropriate function.

Equivalently, the multivariate process X is stable if all the eigenvalues of A(k) have modulus less than 1 (Lütkepohl, 2005).

3.1.1 MVAR estimators

Algorithms for fitting MVAR models can be separated in two big groups, Least Squares models as Yule Walker equations and non-Least Squares as Vieira Morf lattice algorithms. Lattice algorithms, can simultaneously calculate the forward and backward model coefficients given a set of special reflection coefficients. The forward linear predictor estimates the sample $u(n)$ from the previous m samples while the backward prediction attempts to predict the $u(n+M-1)$ sample given the next M elements. Below, we denote the estimated reflection coefficients $\widehat{\Phi}(k)$ and $\widehat{\Psi}(k)$ as referred in (Brockwell, Dahlhaus, & Trindade, 2005).

$$\widehat{\Phi}(k) = \left(\frac{1}{n}\sum_{t=1}^{n+k} \hat{\varepsilon}_J(t)\hat{\eta}_{J^*}(t-k)'\right)\hat{V}_{J^*}^{-1}$$

$$\widehat{\Psi}(k) = \hat{V}_{J^*}\widehat{\Phi}(k)'\hat{U}_J^{-1}$$

The $\widehat{\Phi}(k)$and $\widehat{\Psi}(k)$ are the estimated reflection coefficients where $\hat{\varepsilon}_J$ is the empirical forward prediction error, the $\hat{\eta}_{J^*}$ is the empirical backward prediction error, the $\hat{V}_{J^*}$ is the covariance matrix of the backward error vector, the $\hat{U}_J^{-1}$ is the inverse covariance matrix of the forward error vector and the $k \in K = \{1, \dots, p\}$ is the time lag of the vector autoregression process.

A variety of different estimators have been formulated by modifying the equations that estimate the reflection coefficients, such as Nuttall-Strand, Vieira Morf and Burg. The Vieira Morf estimators appear to be more effective and give higher Gaussian likelihoods with less variability compared to other techniques. An additional property of these estimators is that simultaneously minimizing weighted forward and backward prediction errors. Thus, we decided to focus on this algorithm to calculate the coefficients (Brockwell et al., 2005).

3.1.2 Model Order Selection for the MVAR models

The main parameter in VAR model fitting is the model order. We select the model order that minimizes the criterion below (Cr) (Lütkepohl, 2006). The standard form of the model order criteria (or information criterion) is:

$$Cr(m) = \log\det\left(\sum\nolimits^{\sim}(p)\right) + c_T\varphi(p)$$

$\sum(p)$ is the residual (or noise) covariance matrix for a model of order p and$logdet\sum\nolimits^{\sim}(p)$measures the estimated fit of the model (prediction error). We could also call it the entropy rate. It decreases when p increases. The term $\varphi(p)$ represents the number of parameters which have to be estimated and C_T is a variable that depends on the sample size T. Akaike Information Criteria (AIC), Schwartz-Bayes Criterion (SBC), Akaike's Final Prediction Error (FPE) and Hannan-Quinn Criterion (HQ) are some of the most popular information criteria. All of them were used in this research. The ideal model could be the one which its model order minimizes both terms, a model that is parsimonious and accurate with data modeling.

Akaike Information Criterion

$$AIC(p) = \ln\left|\sum\nolimits^{\sim}(\mathrm{p})\right| + \frac{2}{\hat{T}}pM^2$$

Akaike's Final Prediction Error

$$FPE(p) = \left|\sum\nolimits^{\sim}(\mathrm{p})\right| + \frac{\hat{\mathrm{T}} + \mathrm{Mp} + 1}{\hat{T} - Mp - 1}$$

And its logarithm

$$\ln\big(FPE(p)\big) = \left|\sum\nolimits^{\sim}(p)\right| + Mln\left(\frac{\hat{\mathrm{T}} + \mathrm{Mp} + 1}{\hat{T} - Mp - 1}\right)$$

Schwartz – Bayes Criterion

$$SBC(p) = \ln\left|\sum\nolimits^{\sim}(\mathrm{p})\right| + \frac{\ln(\hat{T})}{\hat{T}}pM^2$$

Hannan-Quinn Criterion

$$HQ(p) = \ln\left|\sum\nolimits^{\sim}(\mathrm{p})\right| + \frac{2\ln(\ln(\hat{T}))}{\hat{T}}pM^2$$

The essential difference between the criteria is how each one penalizes the increase in the model order. The concept behind heavy penalization of high model orders is to improve forecasting performance by reducing over-fitting. Some features that we should have in mind

for the criteria above are that AIC and FPE outperform SBC and HQ in small sample sizes and SBC penalizes more heavily larger model orders than the others. Also, HQ dispose intermediate penalization between SBC and AIC while show a clear minimum (Lütkepohl, 2006).

The "frequency resolution" is determined by the model order because the model order controls the number of modeled frequency components. We can observe p/2 frequency components between each pair of variables (Schlögl, 2006a), so the optimal lower bound on the model order should be twice the number of the expected frequencies plus one. Additional, considering the physiological system and the time between the underlying brain processes, we expect the model order to be greater than the time lag in seconds of the processes multiplied by the sampling rate in Hz, namely $p \geq \tau F$.

Generally, the selection of the model order presupposes combination of these information with expectations from the bibliography. Through one of the next steps, the model validation, we define the quality of our model fit and revise our model characteristics (among other, selection of a different model order) until the data is adequately modeled.

3.1.3 Window length selection

The length of the sliding window was selected according to the equation[3]:

$$W \geq 10 \left(\frac{Mp}{N}\right)$$

Where W is the window length, p is the model order, M is the number of Independent Components and N is the number of trials. This equation comes from the following statement. According to (Schlögl& Supp, 2006)(Korzeniewska, Crainiceanu, Kuś, Franaszczuk, & Crone, 2008) there must be a sufficient number of data points available to accurately fit the model. We have Mp coefficients to estimate for a multivariate model which requires minimum of Mp data samples. In addition, there must be at least 10 times that many data points to ensure an unbiased fit.

$$WN \geq 10Mp$$

[3] As Makoto Miyakoshi stated in his pipeline (https://sccn.ucsd.edu/wiki/Makoto%27s_preprocessing_pipeline), the equation used in SIFT's function est_checkMVARParams() line 85 for testing the 'window length' is wrong and till the publishing of this thesis in not corrected by the authors of the toolbox. Here we refer to the correct form of the equation. The interested reader should correct the script of the equation on his own according with the author's guidance in the link.

3.1.4 Model Validation

Checking the residuals

$$X(n) = \sum_{k=1}^{p} A(k)X(n-k) + U(n) \quad (Eq.1)$$

The matrix $A(k)$ with the model coefficients describe the linear interaction at lag k from $\chi_j(n-k)$ to $\chi_i(n)(i,j=1,\dots,M)$. For these model coefficients we can obtain the residuals$U(n) = [u_1(n),\dots,u_M(n)]^T$ that they should be uncorrelated if we have adequately modeled the data. We check the correlation structure (or the whiteness) of the residuals with testing the autocorrelation coefficients. If the coefficients up to a lag $h$are small enough, it is ensured that we cannot reject the null hypothesis (definition below) of white residuals at some significance level(Delorme et al., 2011a).

Firstly, the lag $h$autocovariance matrix of the residuals is given by$C_h = E[U_n U_{n-h}]$.

$$C_h = \begin{bmatrix} Cov(X_1, X_{1-h}) & \dots & Cov(X_1, X_{n-h}) \\ \vdots & \ddots & \vdots \\ Cov(X_1, X_{n-h}) & \dots & Cov(X_n, X_{n-h}) \end{bmatrix}$$

We define the lag h autocorrelation matrix $R_{\mathrm{h}} = D^{-1}C_h D^{-1}$ where D^{-1} is a diagonal matrix of which its elements are the square root of the diagonal elements of C_0

The autocorrelations up to a lag h are defined as $\boldsymbol{R}_h = (R_1,\dots,R_h)$

The general idea is testing if the null hypothesis (the residuals are white) $H_0: \boldsymbol{R}_h = (R_1,\dots,R_h) = 0$ or the alternative $H_1: \boldsymbol{R}_h \neq 0$ is true.

The simplest test, based on asymptotic properties of univariate white noise processes involve rejecting the hypothesis that U is white noise at the 5% level if $|R_h| > \pm 2\sqrt{\hat{T}}$ for any lag h for $\hat{T} = TN$ is the total number of samples. The probability of a coefficient exceeding the 5% significance bounds:

$$\rho = \frac{count(|\boldsymbol{R}_h| > \pm 2\sqrt{\hat{T}})}{count(\boldsymbol{R}_h)}$$

If $\rho < 0.05$we cannot reject the null hypothesis at the 0.05 level and we accept that the residuals are not correlated and white.

The simple asymptotic ACF test in small samples may be conservative (reject the null hypothesis less often than indicated) and lead to misleading results (Lütkepohl, 2005). For this reason we propose some alternatives, for testing of the residuals, through portmanteau test statistics: Box-Pierce (BPP), Ljung-Box (LBP), Li-McLeod (LMP). Each of these tests follows a χ^2-distribution. Also, we obtain a ρ-value by comparing the test statistic with the cumulative distribution function of this distribution.

The Box Pierce (BPP) test is the original portmanteau test. For small samples its distribution diverges from the asymptotic distribution and this can make it overly conservative.

$$BPP_h = \hat{T} \sum_{l=1}^{h} tr(C_l' C_0^{-1} C_l C_0^{-1})$$

The Ljung-Box (LBP) test improves small sample properties but inflates the variance of the test statistic. It is more sensitive with significance levels somewhat larger than expected in large samples.

$$LBP_h = \hat{T}(\hat{T}+2) \sum_{l=1}^{h} (\hat{T} - l)^{-1} tr\,(C_l' C_0^{-1} C_l C_0^{-1})$$

The Li-McLeod (LMP) it has better small properties than BPP without inflating its variance. The statistical power of LMP and LBP is almost identical while LMP is slightly more conservative.

$$LMP_h = \hat{T} \sum_{l=1}^{h} tr\,(C_l' C_0^{-1} C_l C_0^{-1}) + \frac{M^2 h(h+1)}{2\hat{T}}$$

Checking the consistency and stability of the model

As we would like to examine of what fraction of the correlation structure of the original data is captured by our fitted MVAR model, we calculated the percent consistency. We compared the real data with the simulated data segments of equal dimensions. In each window we computed all auto-correlations and cross-correlations between all the variables up to a predetermined lag. The statistical consistency between the correlation structure of the real data and of the simulated data can be measured by the percent consistency (PC) measure:

$$PC = \left(1 - \frac{\|R_s - R_r\|}{\|R_s\|}\right) \times 100$$

A PC value near 0% indicates a failure to model the data. When the PC value is near 100%, this denotes that the simulated model is able to generate data with almost identical characteristics as the original data.

In exact terms, a VAR process is stable if its reverse characteristic polynomial has no roots in or the complex unit circle. Precisely,

$$\det(I - Az) \neq 0 \text{ for } |\,z\,| \leq 1$$

In other words, an M-dimensional VAR[p] process is stable if all the eigenvalues of the $[Mp \times Mp]$ coefficient matrix A have absolute value less than 1(Lütkepohl, 2005). Thus, the stability index we used is the ln of the largest eigenvalue λmax of the coefficient matrix A:

$$SI = \ln |\lambda_{max}|$$

If the SI is negative ($SI < 0$), the VAR[p] process is stable. A stable process is a stationary process, so it is sufficient to check only the stability.

3.2 Granger causality in MVAR modeling

Let the V represent the set of all the EEG variables: $V = \{1,2,\dots,M\}$

$$X^V(t) = \sum_{k=1}^{p} A(k)X^V(t-k) + U(t) \quad (Eq.1)$$

We calculate the mean-square prediction error when x^i is predicted from the past values of x^V up to the specified model order:

$var(x_t^i|x^V) = var(u_t^i)$where$x^V = \{x_{t-k}^V, k \in \{1,\dots,p\}\}$ denotes the past of x_t

We exclude the variable j from the set of variables and refit the model:

$$X^{V\setminus j}(t) = \sum_{k=1}^{p} \bar{A}(k)X^{V\setminus j}(t-k) + \bar{U}(t)$$

With mean square prediction error:

$$var(x_t^i|x^{V\setminus j}) = \overline{var}(u_t^i)$$

Generally, $var(u_t^i) \geq \overline{var}(u_t^i)$.

That means that the fitted model without the variable j will be more accurate to predict the variable x^i than the fitted model with all the variables (included$j$). This is one important part of the multivariate Granger causality definition.

Definition:
Let i and j be two variables of V. Then x^j Granger causes x^i if and only if:
$var(u_t^i) \geq \overline{var}(u_t^i)andA_{k,ij} \gg 0 \; for \; some \; k \in \{1,\dots,p\}$

$$F_{ij} = ln\left(\frac{var(x_t^i|x^i)}{\overline{var}(x_t^i|x^i, x^j)}\right)$$

The non-negative quantity F defines the process j to process i and increases to the degree to which the past of process j "granger-causes" (conditionally explains) the future of process i time series (Granger, 1969)(Geweke, 1982).

In the frequency domain, we obtain the Fourier-transform of our VAR[p] coefficient matrices$A(f)$.

$$X(t) = \sum_{k=1}^{p} A(k)X(t-k) + U(t) \quad (Eq.1)$$

$$U(t) = \sum_{k=0}^{p} \hat{A}(k)X(t-k)$$

We use Fourier transformation:

$$U(f) = A(f)X(f) \text{ where } A(f) = \textstyle\sum_{k=0}^{p} \hat{A}(k)e^{-i2\pi fk}$$

Multiplying by $A(f)^{-1}$ we have $X(f) = A(f)^{-1}U(f) = H(f)U(f)$

where $X(f)$ is the spectral matrix of the multivariate process, $U(f)$ is a matrix of random sinusoidal shocks and $H(f)$ is the transfer matrix of the system.

Definition:
Let i and j be two variables of V. Then x^j Granger causes x^i if and only if:

$$A_{ij} \gg 0 \; for \; some \; frequency \; f$$

As a result we test for the non zero coefficients of $|A(f)|$and by this come a group of GC estimators called Partial Directed Coherence measures (PDC).

There is a direct relationship between time-domain and frequency domain on Granger causality. The time domain GC estimator F_{ij} and the frequency domain GC estimator $W(f)_{ij}$hold the below equivalency:

$$F_{ij} = \int_0^{\frac{F}{2}} W(f)_{ij} \, df$$

The Granger Causality extends through the MVAR models and the Fourier transformation to get the transfer, spectral density matrices, ordinary and partial coherences(Delorme et al., 2011a). Through frequency domain representation of bivariate GC and measures of directed conditional multivariate dependence as the DTF and PDC the brain network dynamics are described. To study the causal dynamics of non-stationary EEG channel time series, we implement filtering, locally stationary sliding windows and spectral matrix factorization. These approaches can be used to explore the time- and frequency-dependent dynamics of directed information flow or causality during cognitive information processing between brain sources.

3.3 MVAR modeling with SIFT toolbox

Source Information Flow (SIFT) is an open-source Matlab (The Mathworks, Inc.) toolbox for modeling and visualizing information flow between sources of electrophysiological data(Mullen, 2014). The data must be first separated into maximally independent processes using Independent Component Analysis (ICA) to apply them the six modules, as follows:

(1) data preprocessing, that contains functions for normalization, downsampling, detrending, and other standard preprocessing steps
(2) model fitting and connectivity estimation, that consists of adaptive MVAR modeling approaches (ARfit, Group Lasso, Ridge regression, SCSA, Vieira Morf). From the fitted model, the user can chose to estimate spectral power, coherence, and frequency-domain connectivity.
(3) statistical analysis, with surrogate statistics (phase-randomization and bootstrap statistics) for all measures, and analytic statistics for partial directed coherence and directed transfer function measures.
(4) visualization, with novel routines for interactive visualization of information flow dynamics and graph-theoretic measures across time, frequency, and anatomical source location.

The main characteristic of SIFT comparing to other toolboxes is that the dynamical modeling is performed at the level of sources rather than between surface EEG signal channels. That gives the advantage of minimizing the risk of misidentifying network events

resulting from mixing brain and non brain sources (arising by volume conductions or other artifacts). Transient dynamic network events between spatially static components could be detected from this toolbox.

3.4 Clustering

Spatially and functionally clustering was used through the EEGlab toolbox to define the cortical regions of interest (ROIs) for the later connectivity analysis. We did not take the raw EEG signal from the channels for the clustering procedure. Instead, we followed a preprocessing pipeline through filtering and ICA decomposition. In the Independent Component Analysis some filters (from EEGLAB[4] toolbox) produce the maximally temporally independent signals available in the channel data with a linear change of basis. These are, in effect, information sources in the data whose mixtures, via volume conduction have been recorded at the scalp channels.

Information from the equivalent dipole fitted to each IC, the event related potential (ERP), the topographical scalp map of the IC, the Event Related Spectral Perturbation of the IC (ERSP)(Makeig, 1993) andtheInter Trial Coherence (ITC) was used to extract homogenous clusters with similar functional characteristics.

The equivalent dipole fitted to each component was estimated with the use of a non-linear optimization technique using a spherical model. The goal of the inverse problem solving is to find some number of equivalent current dipoles (like small batteries), whose summed projections to the scalp nearly resemble the observed scalp distribution. The event-related potential (ERP) is the electrophysiological response to any stimulus that could evoke sensory, cognitive or motor action. The EEG reflects simultaneously a lot of brain processes, so the brain response to a single stimulus is not usually visible in the EEG recording in a single trial. To estimate the wavelength of the ERP, we must average the results from many trials causing random brain activity to be averaged out. An experimental task could create several ERP components in the EEG signal consecutively, for example N100 denotes the Negative ERP component around 100 msec after the onset of the stimulus while P300 denotes the Positive ERP component around 300 msec.

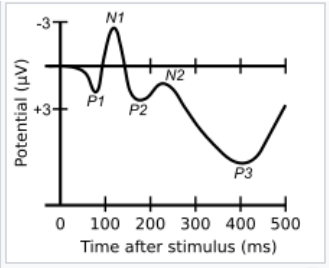

A waveform showing several ERP components, including the N100 (labeled N1) and P300 (labeled P3). Note that the ERP is plotted with negative voltages upward, a common, but not universal, practice in ERP research

FIGURE 3 EVENT RELATED POTENTIAL (SOURCE: WIKIPEDIA)

The topographical scalp maps we took into account to form the clusters describe the distribution of electrical activity across the brain as measured from the EEG channels. The ERSP measures average dynamic changes in amplitude of the broad band EEG frequency spectrum as a function of time relative to an experimental event. That is, the ERSP measures the average time course of relative changes in the spontaneous EEG amplitude spectrum induced by a set of similar experimental events. These spectral changes typically involve more than one frequency or frequency band, so full-spectrum ERSP analysis yields more information on brain dynamics (Makeig, 1993).

For explaining the Inter-trial coherence let's start with the definition of time-frequency analysis, where the ITC measure belongs (Nash-Kille & Sharma, 2014). Time-frequency analysis adopt a different perspective on the evoked response from the traditional time-only analyses where component peaks are averaged, while the remainder of the evoked potential signal is considered to be noise and disregarded. In time-frequency analyses, we

[4] https://sccn.ucsd.edu/wiki/Chapter_09:_Decomposing_Data_Using_ICA

focus on brain oscillations, which can be detected using a time-frequency decomposition of the EEG. When the waveform of the EEG is interrupted by a stimulus event, the distribution of EEG phase becomes “phase-locked” to that event (Makeig, Debener, Onton, & Delorme, 2004) and this phase synchronization of brain oscillations can be determined by computing phase relations across single trials. Phase synchronization of brain oscillations within and between cortical areas is a fundamental mechanism involved in information processing and has been found to be critical for feature-binding and other cognitive processes (Tass et al., 1998) (Palva, Palva, & Kaila, 2005). Inter-trial coherence (ITC) is a measure that is computed from single trial EEG, which reflects the temporal and spectral synchronization within EEG, elucidating the extent to which underlying phase-locking occurs. Thus, ITC provides a direct measure of cortical synchrony that is not available in the aggregate evoked response waveform. All this information from these measures is combined to extract the clusters and subsequently the ROIs of our research.

3.5 Source Localization

For the estimation of the source localization of the brain activations, we should solve the forward and the inverse problem with specific algorithms. For forward and inverse distributed source imaging,we used theDistributed Source Imaging (DSI)toolbox that combines the ‘Head model’ toolbox and the Recursive Sparse Bayesian Learning inverse filtering code(Ojeda, Klug, Kreutz-Delgado, Gramann, & Mishra, 2019). We have used forward modeling routines from the ‘HeadModel’ toolbox for x,y,z, which is open-source and can be freely downloaded from https://github.com/aojeda/headModel. The forward model function coregistered the channel positions to a head model template based on the standardized MRI MNI Colin27three layer Boundary Element Models (Holmes et al., 1998) and computed the lead field matrix through OpenMEEG template (Gramfort Alexandre, Papadopoulo Théodore, Olivi Emmanuel, & Clerc Maureen, 2010). The electrical lead field matrix was computed for the three BEM layers, “relating the conduction of electrical fields generated by current dipoles from the cortical mesh (bottom layer) to the top of the skin (outer layer) where the field potential is recorded by scalp electrodes”(Courellis, Mullen, Poizner, Cauwenberghs, & Iversen, 2017).

The Recursive Sparse Bayesian Learning (RSBL) filtering algorithm used for inverse modeling(Ojeda et al., 2019). Solving the ‘inverse model’, we localize the current source inside the fixed brain source we made previously and transform scalp EEG data to distributed cortical source estimates. More specifically, we find the equivalent electric dipole whose projections to the brain most nearly correspond to the observed scalp map distribution. We chose the RSBL algorithm because ‘it induces the segregation of the electrical activity into a few maximally independent components’ with anatomical projections while minimally overlapping artifact activity. It reduces the artifacts without significantly deforming the epochs of the data, in contrast with other algorithms (Ojeda et al., 2019). At the same time, we reduce the source activity from the cortical space to the ROI space taking the mean of the source values within it (estimate the current localized at each grid-point in the head model within a given ROI). As a result, each ROI has a single time series that represent the dynamics taking place in it. For further analysis, we select the ROIs that include the centroids or were approximately neighboring with the centroids from the clustering conducted before.

4. Brain Connectivity

Brain Connectivity may reflect several different aspects of brain organization. Structural, functional and effective connectivity attempt to group these aspects in distinct categories(Karl, 1994). *Structural connectivity* refers to a network of anatomical (direct or indirect axonal-dendritic) connections linking neurons. *Functional connectivity* describes statistical dependence (i. e. measuring correlation, covariance, spectral coherence, phase locking) between all brain regions of a system, regardless whether these elements are connected directly or not. This kind of connectivity is highly time-dependent but it cannot provide identification of asymmetric information transfer or directional effects between brain areas. Functional connectivity can be estimated through computing cross-correlations in the time frequency domain or spectral coherence. *Effective connectivity* provides the identification of asymmetric information transfer mentioned above and refers to causal dependencies of one neural element over another. We will choose to deepen on the last type of connectivity as it is usually better for understanding the functional brain segregation (one of the principles of brain organization). Effective connectivity mediates the influence that one neuronal system exerts on another.

For estimating effective connectivity various techniques are proposed(V. Sakkalis, 2011). One widely adopted technique is estimation through the time-series analysis that based on adaptations of the concept of Granger causality. Transfer entropy(Schreiber, 2000) detects directed exchange information between two systems taking into account how the state of one element effects the state of another. The measures based on Granger causality and transfer entropy are the Directed Transfer function and the Partial Directed Coherence. These measures are defined in the Multivariate Autoregressive Modeling framework.

Structural connection patterns constrain a lot the cortical circuits and therefore the functional and effective connectivity. But also temporal activations in functional or effective connectivity may mirror changes in anatomic-structural variables. Given these links for the brain connectivity, it is likely that structural characteristics relate with functional interactions.

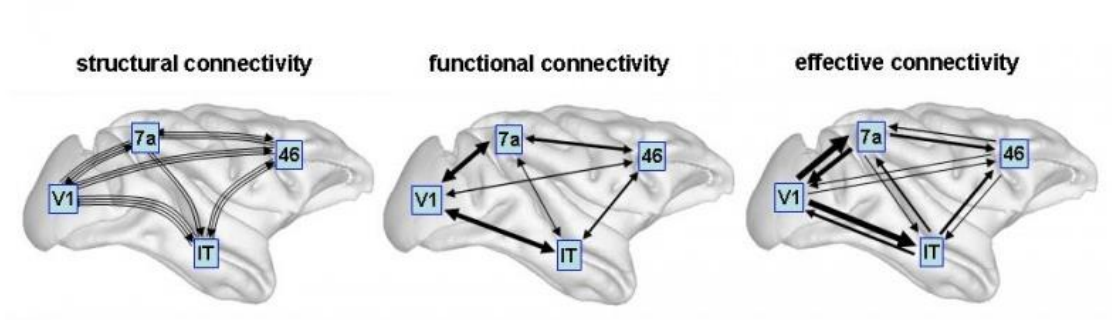

FIGURE 4 SKETCHES ILLUSTRATE STRUCTURAL CONNECTIVITY (FIBER PATHWAYS), FUNCTIONAL CONNECTIVITY (CORRELATIONS) AND EFFECTIVE CONNECTIVITY (INFORMATION FLOW) AMONG BRAIN REGIONS IN MACAQUE CORTEX (HONEY, KÖTTER, BREAKSPEAR, & SPORNS, 2007).

Segregation and integration are two potential principals that link anatomical, functional and effective connectivity (Tononi, Sporns, & Edelman, 1994). The existence of specialized neurons and brain areas grouped to form segregated cortical areas called 'segregation'. The activation of distributed neuronal populations and therefore enabling the appearance of contiguous cognitive states called 'integration'. The interaction between segregation and integration generates information that is highly diversified and highly

integrated, thus creating patterns of high complexity. The application of network analysis techniques allows the comparison of high complexity brain connectivity patterns.

Brain connectivity patterns derive from network analysis techniques and can be represented as matrices or graphs. Structural connectivity is imprinted in a weighted or binary graph. The weighted graph represents connection densities and the binary graph represents the presence/absence of a connection. A full symmetric matrix is formed when we study the functional connectivity. By the values of the matrix are denoted the statistical dependence between two elements (i.e. neurons). Effective connectivity constructs a full non symmetric matrix that applying a threshold creates a binary directed graph. A binary graph could be created from a full symmetric matrix also.

The construction of the brain graph requires the use of a multivariate autoregressive model on the EEG data and a function that will be used as an estimator of the intensity of the activity flow between the brain regions. Direct Transfer Function is a function among others that will be the one we will use in this thesis based on the Granger causality principle between time series (Granger, 1969) and the spectral properties of the initial signals.

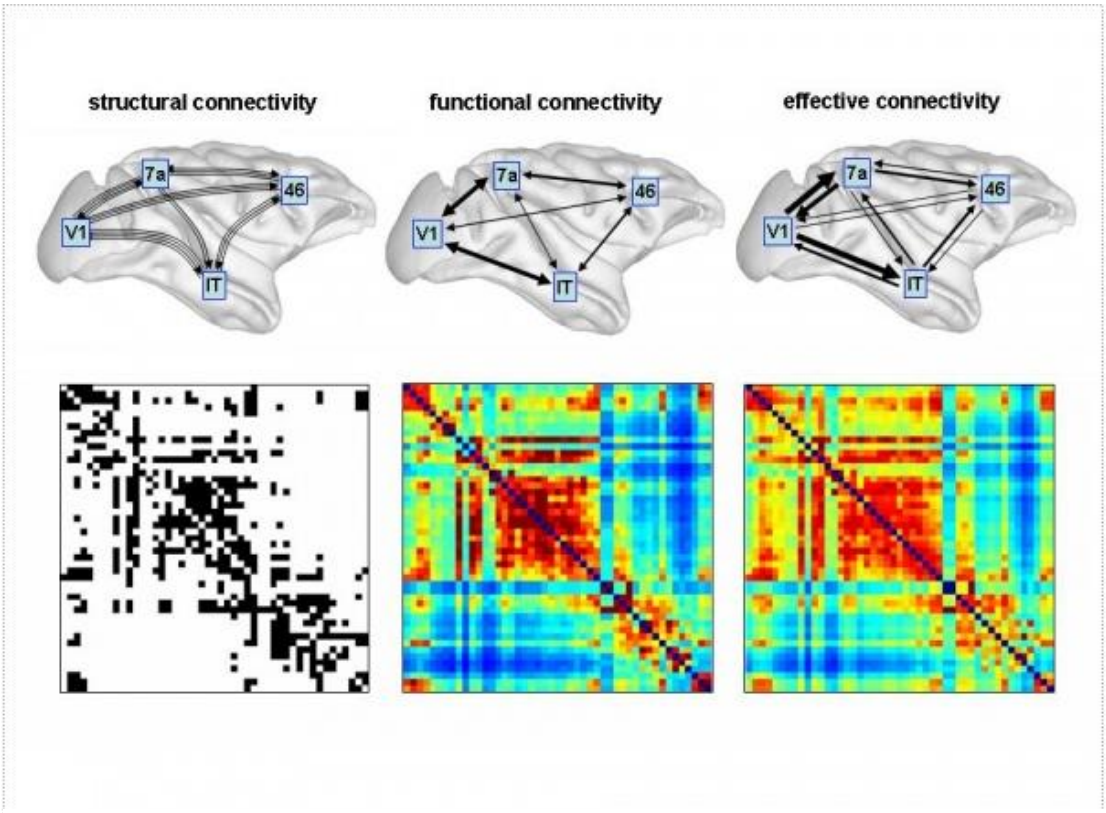

FIGURE 5 MATRICES SHOW BINARY STRUCTURAL CONNECTIONS FROM STRUCTURAL CONNECTIVITY (LEFT), SYMMETRIC MUTUAL INFORMATION FROM FUNCTIONAL CONNECTIVITY (MIDDLE) AND NON-SYMMETRIC TRANSFER ENTROPY FROM EFFECTIVE CONNECTIVITY (RIGHT). DATA WAS OBTAINED FROM A LARGE-SCALE SIMULATION OF CORTICAL DYNAMICS(Honey, Kötter, Breakspear, & Sporns, 2007).

4.1 Directed Transfer Function (DTF)

Each graph has to be estimated from the EEG data. In a brain network, each vertex is a brain area or Region of Interest (ROI) and each edge corresponds to statistical dependence in the activation between two areas. A lot of techniques measure both the linear and

nonlinear dynamic coupling between different brain regions. When these methods apply in different frequency bands constitute indices of cerebral engagement in cognitive tasks.

For the analysis of the relations between brain structures we have applied a multichannel model, which takes into account all signals simultaneously, not pair-wise. The multichannel approach avoids the general disadvantage of pair-wise analysis, which in certain cases can lead to incorrect conclusions especially when some channels are fed from common signal sources, as is very likely in neurobiological systems. Additionally, the multichannel model creates a common base with regard to the whole system providing an absolute scale for comparison of quantitative results. The Directed Transfer Function DTF (Kaminski & Blinowska, 1991) based on the multichannel (multivariate) autoregressive (MVAR) model is an estimator of the intensity of activity flow between structures depending of frequency of the signal. The high value of DTF indicates the information flow between two given brain areas. Also, we should notice that the non-normalized DTF function is equivalent to the Granger causality measure (Kamiński, Ding, Truccolo, & Bressler, 2001). DTF in some cases may not easily differentiate between the direct and the indirect connections via mediating structures, so researchers attempted to create a new measure to estimate direct causal relations between signals. By multiplying DTF by partial coherence we emphasize only in the direct connections. The function direct Directed Transfer Function (dDTF) combines information about direction of influence in one measure (distinguish between direct and indirect connections while minimizing the indirect connections). Estimation of the direction of the EEG flow by means of dDTF (or DTF) relies on the difference of phases between signals (Korzeniewska, Mańczak, Kamiński, Blinowska, & Kasicki, 2003).

4.2 Graph Theory

Measures of graph theory and other mathematical network science tools have been applied aiming to understand the complexity of the brain network(Colombo, 2013)(Fornito, Zalesky, & Bullmore, 2016). Brain graphs are composed from neural elements (neurons or brain regions) and their interconnections (synapses or pathways or statistical dependencies), also called nodes and edges respectively. The simplest form of the graph's topology can be summarized in the form of an adjacency matrix with binary or weighted elements describing the presence or the absence of an edge or a directed edge.

One analysis approach focusing on the network's topological features such as the path lengths (distances), subgraphs (motifs), clustering coefficients, vertex and edge centrality. This approach requires the suitable random graph model accompanied with the appropriate null hypothesis. These random graph models are not uniquely defined, they differ but they preserve some subsets of structural parameters, i.e. edge randomization techniques with preserved vertex degrees. The detection of network communities through the observation of the graph's eigenspectrum is another technique that could be applied to brain connectivity datasets. Another analysis approach focus on the three dimensional structure of brain networks that include for example measuring wiring length or volume(Wen & Chklovskii, 2005).

According to the first analysis approach, we decided to estimate some basic metrics to compare the constructed subjects' graphs(Vangelis Sakkalis, Tsiaras, & Tollis, 2010). Centrality measures are the local measures detecting which vertices are the most relevant to the organization and functioning of a network, for example node betweenness centrality degree and node strength. Node betweenness centrality (BC) degree is the fraction of all

shortest paths in the network that contain a given node. The equation is defined below where σ_{xy} is the total number of shortest paths from node x to node y and $\sigma_{xy}(u)$ is the number of those paths that pass through u.

$$BC(u) = \sum_{u \neq x \neq y} \frac{\sigma_{xy}(u)}{\sigma_{xy}}$$

Node strength is the sum of weights (SW) of links connected to the node. In directed networks, the in-strength is the sum of inward link weights and the out-strength is the sum of outward link weights("Node Degree and Strength," 2016). The out-strength and the in-strength value will be referred also as 'Outflow' and 'Inflow' in this thesis because of the different appellation used by Sift toolbox.

$$SW = \frac{1}{n-1} \sum_{u \neq v} w_{u,v}$$

In order to obtain a better understanding of network's structure and function, networks are often classified into categories. We classify a network by describing essential properties of the network called graph (or network) metrics. Network metrics like clustering coefficient or average shortest path length are chosen to catch the needed information to differentiate graphs into different categories. The average shortest path length (L) is a measure of interconnectedness of the graph and defined as the shortest path between any two pairs $u, v \in V, u \neq v$ of nodes in a network.

$$L = \frac{1}{n(n-1)} \sum_{u,v \in V} d(u,v)$$

We decided to use the dDTF with causal normalization function to create the graph of each subject because it combines the advantages of DTF and partial coherences. Also the new dDTF (or SdDTF) was normalized to all direct transfers between channels (Korzeniewska et al., 2008). We calculate only some representative measures from each group of metrics: the centrality degree, the node strength, the in-strength and out-strength from the centrality measures and the average shortest path of each graph from the graph metrics.

5. Methodology

Below we can see in a diagram the methodology we used and the nine (9) steps of the analysis.

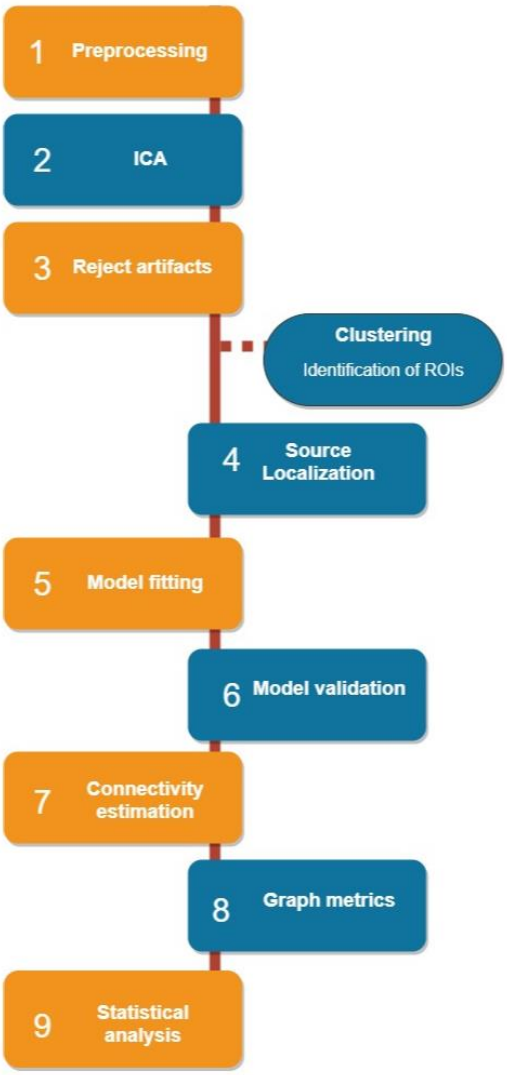

5.1 Dataset description

The data collected from Plymouth University in the U. K. for course credit. Thirty-one students (Mean= 21 years and 2 months, SD= 5.22) with normal or corrected-to-normal vision took part in the training session and in the experiment while the EEG device was recording. They also completed the HFT and TTCT test.

The experiment consisted of three different tasks and lasted 3 hours: (a) an ambiguous perceptual task, (b) a FD-I visuospatial performance task (Hidden Figures Task) and (c) a creativity performance task (Torrance Test of Creative Thinking). Brain activity captured via a wireless Electroencephalogram (EEG) recording device while the eye moves recorded from a synchronized eye-tracking device. In the current study, we focused on the EEG recordings throughout the ambiguous figures experiment along with the results at the HFT test.

An mBrainTrain Smarting EEG device used along with 24 channels at a sampling frequency of 500 Hz with 24-bit resolution. The electrodes applied following the international 10-20 system. Data were recorded from the recording positions FP1, F7, FC1,

C3, T7, CP1, CP5, TP9, P3 and O1 for the left hemisphere along with their right counterparts FP2, F8, FC2, C4, T8, CP2, CP6, TP10, P4, O2 and from the center electrodes Fz, Cz and Cpz. The reference electrode was positioned at FCz and a ground electrode at Fpz. EEG data were recorded using OpenVIBE 0.18 (Renard et al., 2010)and stored using the European Data Format (EDF+) (Kemp & Olivan, 2003)and the General Data Format for biomedical signals (GDF), version 1.25 (Schlögl, 2006b).

We used 100 black-white images from the collection of Snodgrass and Vanderwart (1980): 50 images having two possible interpretations for the bistable condition and 50 images having a single interpretation for the control condition. The images had random order. At the center of the screen, a fixation cross appeared in every trial and the participants were asked to focus their gaze on it for about 800 to 1300 msec. In the next step the image appeared and the participants were instructed to press a button once they perceive the initial interpretation. If an ambiguous image appeared as a stimulus, participants were asked to press the button once again when they figure out the second meaning. With no report of the second interpretation, the trial ended after 5000 msec. An image of closed eyes reminded the participants to blink between trials. Before the experiment, a training session of 10 trials with two preselected images (one from the bistable condition and one from the normal condition) was performed.

The Hidden Figures Test (HFT) estimates the Field Dependence – Independence level of the participants (E. A. Nisiforou & Laghos, 2013)(R. B. Ekstrom, French, Harman, & Dermen, 1976). Participants have to specify which one of the given five simple geometrical shapes is embedded in a more complex pattern. The HFT duration is 24 min and it is equally divided into two parts. According with the manual, the calculation of the HFT score conducted by taking the number of the correct responses minus the number of the incorrect responses. According to this classification, participants were categorized as 14Field Dependent, 7 Field Independent and 8 Field Neutral learners (also, 2 subjects' recordings were partially destroyed). Only the data of the FD and FI participants were analyzed.

5.2 Preprocessing

Channel space data from EEG was conducted using EEGLAB (Delorme & Makeig, 2004). After bandpass filtering (2-65 Hz) using a Hamming window FIR filter and average re-referencing, we corrected the baseline from the data using the time range [-1000 0]. The data were epoched time-locked to three different events: the appearance of the image on the screen, the first button press that indicates the first interpretation of the image and the

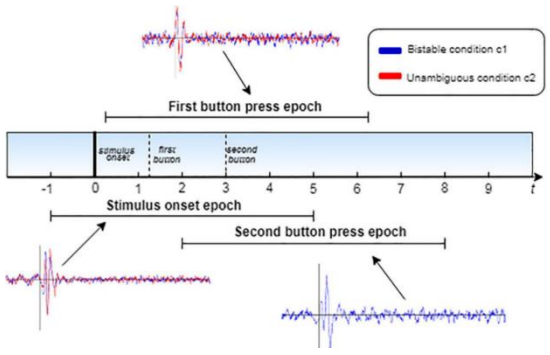

FIGURE 6 SCHEMATIC DIAGRAM OF THE EPOCH EXTRACTION PROCESS. THE PLOTS CORRESPOND TO THE ERPS, AS CALCULATED FOR EACH EPOCH, WHERE THE BLUE LINE CORRESPONDS TO THE BISTABLE CONDITION C1 AND THE RED LINE TO UNAMBIGUOUS CONDITION C2.

second button press the second interpretation of the image. Below there is a schematic diagram denoting the epoch extraction process (Farmaki, Sakkalis, Loesche, & Nisiforou, 2019). The plots correspond to the ERPs, as calculated for each epoch.

After that, the epoched data were decomposed into maximally independent components using theInfomax ICA (implemented for EEGlab toolbox with the algorithm 'runica') (Bell & Sejnowski, 1995). Noise components were identified using IC-label classifier. The classifier implementation is trained in thousands of labeled and unlabeled Independent Components (IC) and classifies each component as brain or non brainsources (eye, muscle, heart, line noise, channel noise and other). From each subject, about ten components with the less percentage of brain sources were removed (Pion-Tonachini, Kreutz-Delgado, & Makeig, 2019).

We checked each component before removing it examining carefully its plot: the scalp topography, the ERP image, the component time series and the activity power spectrum. If a component is classified as a brain component, we should check the scalp topography to look dipolar and residual variance from dipole fitting should be lower than 15 %. The power spectrum (down right) should decrease as frequency increases (follows the behavior of the function $X = 1/f$) and the epoched data will have a visible ERP. To distinguish a brain component from an artifact, for example an eye artifact, we check the scalp topographies to be near eyes and the power to concentrate at low frequencies (below 10 Hz). In addition, another argument is that the ERP shows a very noisy signal without a specific waveform.

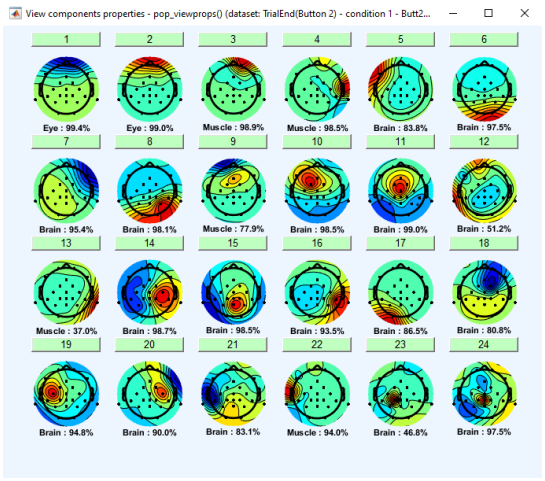

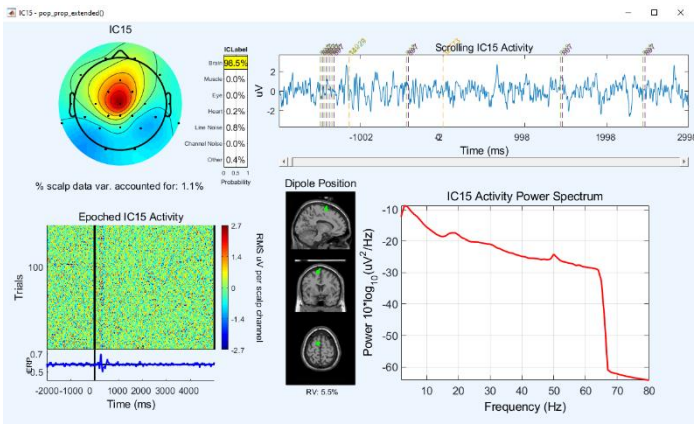

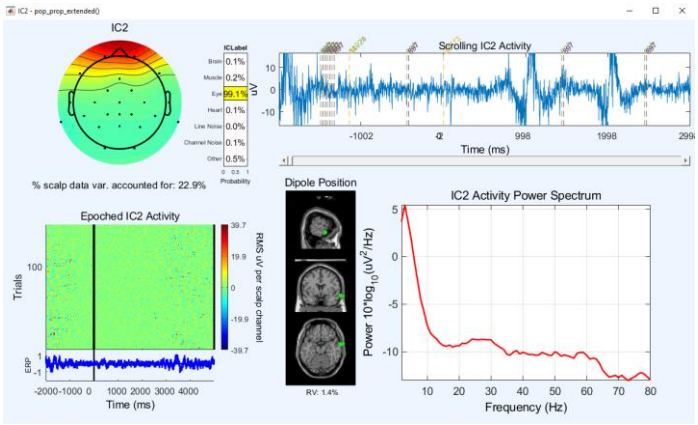

FIGURE 7, 8, 9 EXAMINING IF A COMPONENT CATEGORIZED AS A BRAIN COMPONENT OR AN EYE ARTIFACT (IC-LABEL).

5.3 Clustering – Identification of ROIs

We define the cortical regions of interest (ROIs) using spatially and functionally clustering from the Independent Components (ICs) with the EEGlab toolbox for the connectivity analysis. Information from the equivalent dipole fitted to each IC, the event related potential (ERP), the topographical scalp map of the IC, the Event Related Spectral Perturbation of the IC (ERSP) (Makeig, 1993) and the Inter Trial Coherence (ITC) was used in order to create homogenous clusters with similar functional characteristics (see "Chapter 3.5 Clustering" for more details). We achieved the reduction of the dimensionality of each of the features through Principal Component Analysis (PCA) and following K-means algorithm was used to cluster the ICs into groups. We tested the clustering for eight groups (K=8) to thirteen (K=13) and we choose the most spatially and functionally tight clustering, the one with the nine (9) groups. (Lancaster et al., 2000).

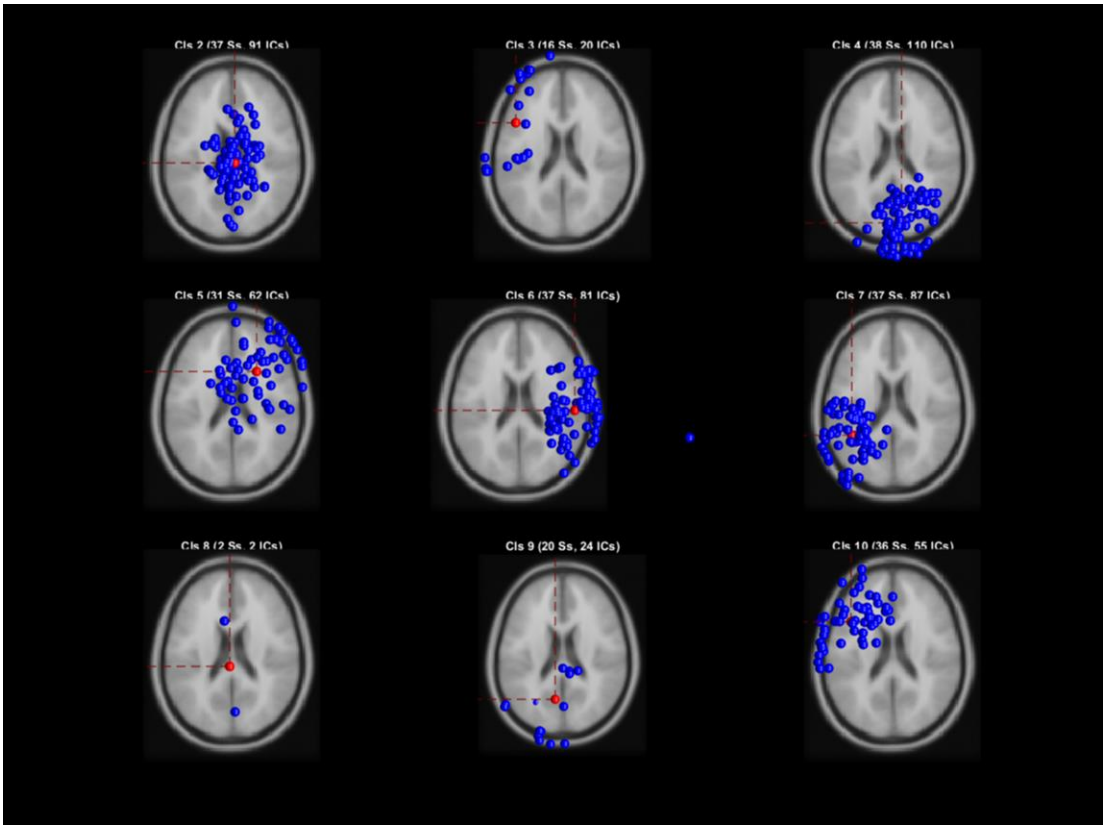

FIGURE 10 AFTER THE CLUSTERING, NINE (9) GROUPS OF COMPONENTS GENERATED TAKING INTO ACCOUNT INFORMATION FROM THE EVENT RELATED POTENTIAL, THE TOPOGRAPHICAL SCALP MAP, THE EVENT RELATED SPECTRAL PERTURBATION AND THE INTER TRIAL COHERENCE.

5.4 Source Localization

We used the Source Localization step (forward and inverse modeling) to localize each Idependent Component (IC) signal into a Region of Interest (ROI) and to calculate the current inside this ROI. After we keep only the ROIs we are interested in that we found them from the previous “Clustering” step.

As we read in the “Chapter 3.4 Source Localization” for forward and inverse distributed source imaging, we used the Distributed Source Imaging (DSI)toolbox that combines the ‘Head model’ toolbox and the Recursive Sparse Bayesian Learning inverse filtering code (Ojeda et al., 2019). Using forward modeling routines, we co-registered the channel positions to a head model and computed the lead field matrix (picture 1, (Litvak et al., 2011)). The lead field matrix relating the conduction of electrical fields generated by current dipoles from the bottom layer of the brain to the skin layer where the electrodes record the field potential.

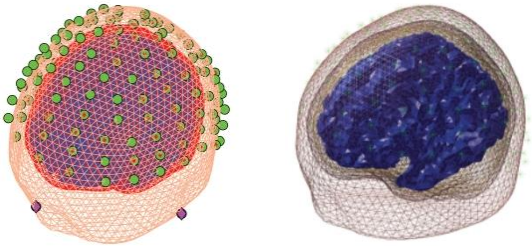

FIGURE 11 THESE FIGURES SHOW THE HEAD MODEL THAT WAS USED TO COMPUTE THE BEM FORWARD SOLUTION FOR THE DATA

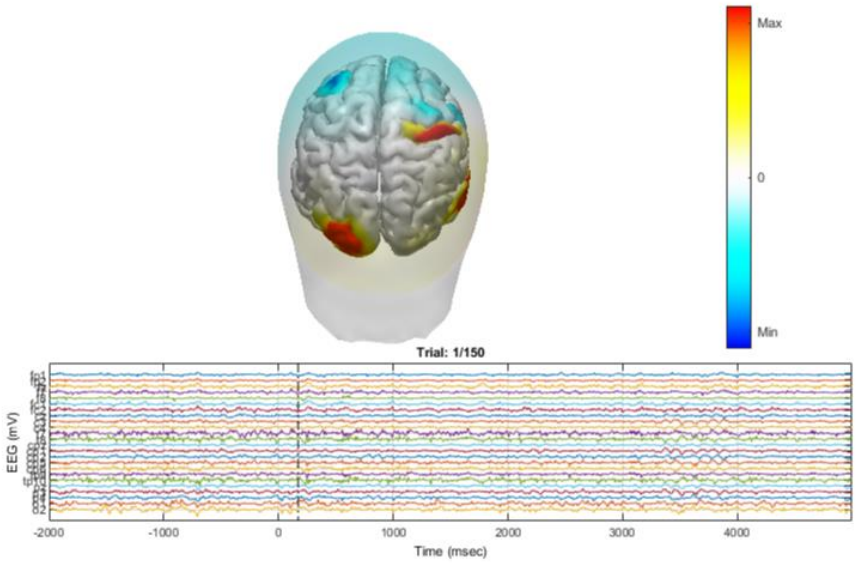

FIGURE 12 THE FIGURE SHOWS THE SOURCE LOCALIZATION OUTPUT FROM THE INVERSE MODELING. FOR EACH ROI (SOURCE) WE CALCULATE A SPECIFIC EEG SIGNAL IN TIME WITH THE RSBL ALGORITHM

For inverse modeling, we used the Recursive Sparse Bayesian Learning (RSBL) (Ojeda et al., 2019) filtering algorithm. Through the solving of the inverse model, we find the

localization of the source inside the lead field matrix we made previously. We transform also all the brain sources inside a ROI in one signal source by taking the mean of the brain sources within each Region of Interest. We take the current localized at each grid-point in the head model within a given ROI and we calculate the average of these values. After this, each ROI has a unique signal. At this step, we distinguish and keep the ROIs for the further analysis that include the centroids from the clustering we did before.

The centroid of each cluster was categorized through the Talairach Atlas and the web application Talairach Applet (Lancaster et al., 2000). The ROIs are in total thirteen (13): right caudal anterior cingulate, right caudal middle frontal, right occipital cuneous, left posterior lobe (fusiform), left parietal inferior (parietal), left posterior lobe - lingual, left posterior lobe - parahimpocampal, right parietal post central, right posterior cingulate, left precentral gyrus frontal, right rostral middle frontal, right superior frontal and left superior temporal gyrus.

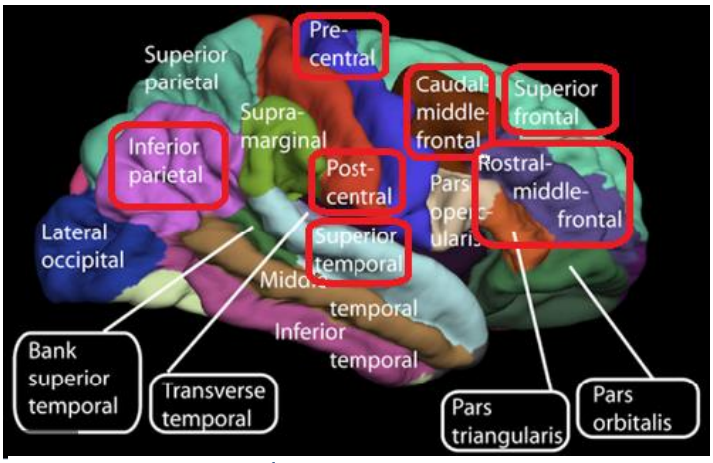

FIGURE 9 REGIONS OF INTEREST (SOURCE: HTTPS://WWW.WIKIWAND.COM/EN/CEREBRUM)

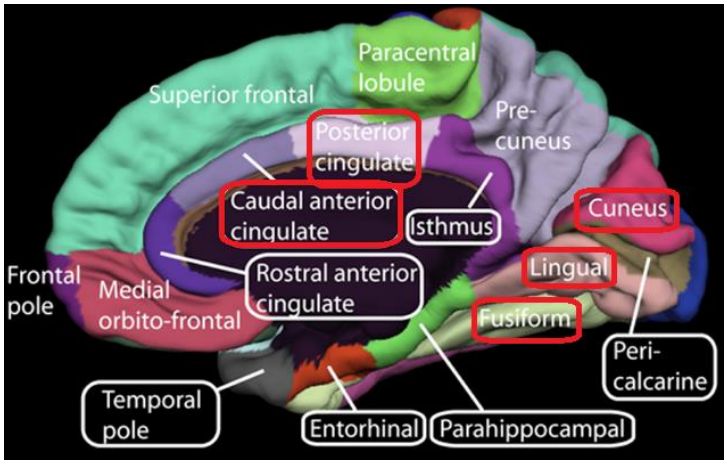

FIGURE 8 REGIONS OF INTEREST 2 (SOURCE: HTTPS://GL.WIKIPEDIA.ORG/WIKI/FICHEIRO:MEDIAL_SURFACE_OF_CEREBRAL_CORTEX__ENTORHINAL_CORTEX.PNG)

6. Results

6.1 Brain Connectivity

The brain activity we kept from each subject was represented from 13 ROIs, as time series. We used SIFT (Delorme et al., 2011b) for Multivariate Autoregressive linear modeling to estimate the multivariate causality between these ROIs. The preprocessing included normalization across time and ensemble. We choose the Vieira-Morf algorithm to construct the MVAR model because it uses a multichannel geometric-mean non-least-squares lattice approach to solve for the model coefficients instead of the common least square approach. The reader could see (Schlögl, 2006a)for a detailed comparison of some estimators with the Vieira Morf.

The optimal order was estimated taking four different estimation criteria: Schwartz-Bayes Criterion (SBC), Akaike Information Criterion (AIC), Akaike's Final Prediction Error (FPE), Hannan-Quinn Criterion (HQ). The whole range of model order 1 to 30 was tested with the criteria above in every subject. The top panel shows the information criteria plotted versus model order. The vertical lines indicate the average optimal model order for each criterion, namely the model order that minimizes each information criterion. AIC and FPE criterion do not seem to exhibit a clear minimum across the specified model range. In contrast, SBC shows a very low value that does not seem to appear reasonable. Thus we decided to take into consideration the 'HQ' criterion as it takes more reasonable values somewhere between the extreme values of the other tests[5]. The lower array of histograms show the distribution of optimal model orders for all windows for each criterion and the vertical lines denote the standard deviations of the distributions.

For each dataset (Trial Start dataset, 1st dataset, 2nd button dataset), we calculate independently the model order. For the Trial Start dataset, the average model order was 10.3, for the 1st button dataset was 10.1 and for the 2nd button dataset, the model order was 12.1. Therefore, we used model order 10, 10 and 12 respectively using rounding. The model order and the window length selection was conducted with the parameter-to-datapoint ratio never exceed 0.1 as is recommended for a well-fitted MVAR model computed with the Vieira Morf algorithm. The window length selected at 0.5 sec and the window step size at 0.03 sec.

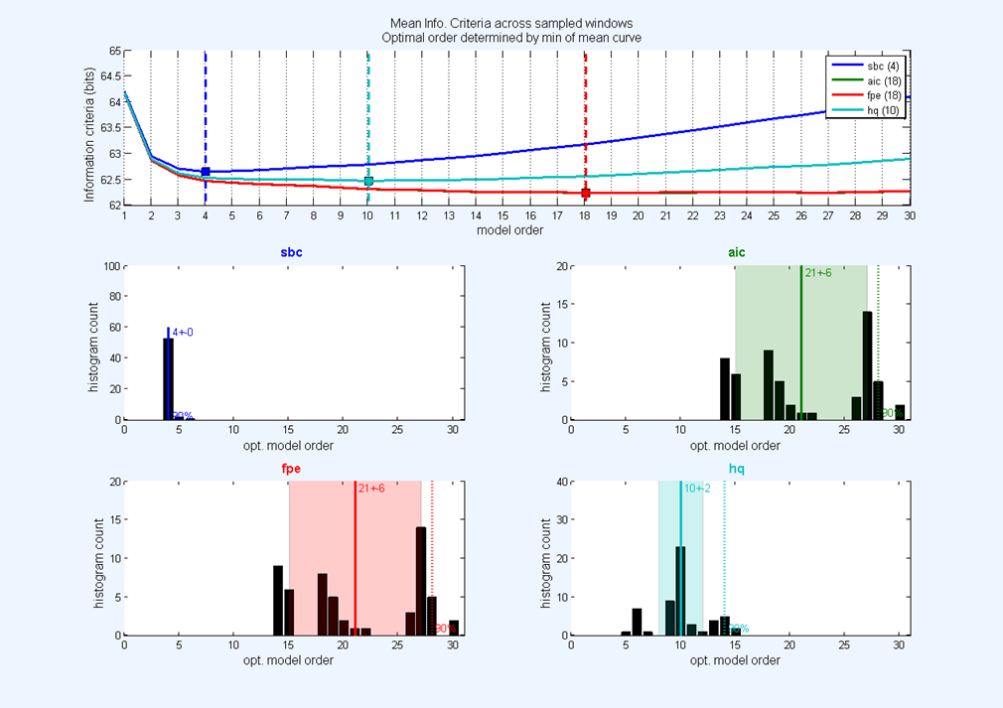

FIGURE 10 RESULTS OF MODEL ORDER SELECTION: THE TOP DIAGRAM PLOTS THE AVERAGE OPTIMAL MODEL ORDER FOR THE SELECTED CRITERIA (INFORMATION CRITERIA VERSUS MODEL ORDER AVERAGED ACROSS WINDOWS). THE LOWER ARRAY OF HISTOGRAMS SHOW THE DISTRIBUTION OF OPTIMAL MODEL ORDERS FOR ALL WINDOWS FOR EACH CRITERION AND THE VERTICAL LINES DENOTE THE STANDARD DEVIATIONS OF THE DISTRIBUTIONS

[5] Another check we did for choosing the right criterion is that we used the model order recommended from the 'HQ' criterion in a small subset of subjects and it passed the validation tests on the contrary with the other model orders suggested from the other tests.

The MVAR model ($X = AX + U$) transforms innovations (random white noise) into observed structured data X. If we have adequately modeled the data, the residuals should be small and uncorrelated (white). Correlation structure in the residuals means there is still some correlation structure in the data that has not been described by our model. Checking the whiteness of the residuals involves testing whether the residual autocorrelation coefficients up to some desired lag h are sufficiently small to ensure that we cannot reject the null hypothesis of white residuals at some desired significance level (the null hypothesis H_o: "the residuals are white", the alternative hypothesis H_1: "the residuals are not white").

The validation tests run independently for every subject and specify if we have appropriately fit our VAR model. The tests we used are checking the whiteness of the residuals, the percent consistency and model stability for each of our windows. The top of the figure shows the results of the whiteness tests as a function of window index. The whiteness test are the Autocorrelation function (ACF) and the Portmanteau tests: Box-Pierce, Ljung-Box and Li-McLeod. In the diagram, we plot for the ACF the probability of an observed ACF coefficient to be within the expected interval for white residuals. Values greater than 0.95 indicate that the residuals are white at the $p < 0.05$ level. In our example, the line of ACF is slightly above the red line so there is increased probability for the residuals to be white. For the Portmanteau tests we plot the p-value of acceptance of the null hypothesis of correlated residuals, namely $1 - p$ is the p-value for rejection of the null hypothesis. Values of the Portmanteau tests greater than 0.05 indicate that the residuals are white at the $p < 0.05$ level. The higher the values are on the level of white significance, the better. As we can see, most of the lines and the dots pass the blue dot line. This indicates that there was no statistically significant correlation structure exposed in the model residuals. In the top right of the figure, all the tests show that not all the windows are white. For the ACF the total number of windows are white (217 from 217 windows are white) and for the Portmanteau tests a little less than the total pass the whiteness test.

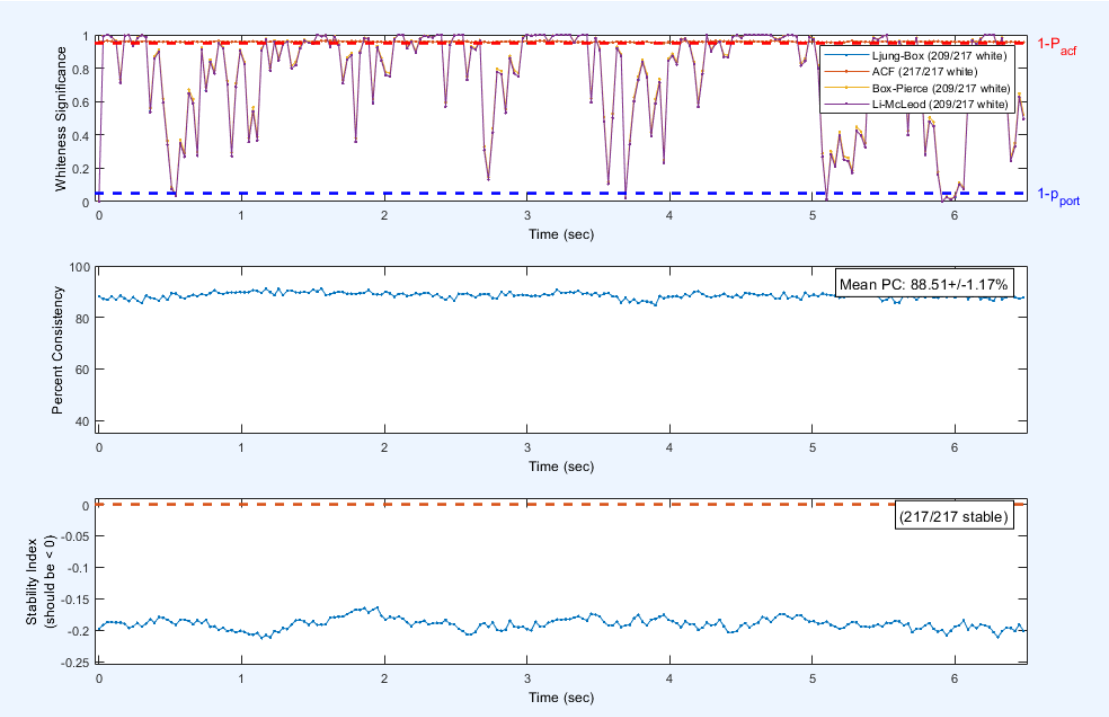

FIGURE 11 THE VALIDATION TESTS (THE WHITENESS SIGNIFICANCE TEST, THE PERCENT CONSISTENCY AND THE STABILITY INDEX)

The middle panel shows the Percent Consistency (PC) plotted versus increasing window index. The PC is reliably high ($\mu = 86.83\%$) suggesting a reasonable model fit. The last panel shows the stability index for each window. Values above or near 0 indicate an unstable and possibly nonstationary model. In our case the stability index is reliably low (-0.12) indicating a stable and stationary model. As a result, examining our tests, the MVAR modeling did not manage with great success in capturing the wholeness of the dynamics exhibited by the brain network but it fitted relatively well in our data.

We computed the connectivity between the ROIs through the DTF function for the gamma, beta, alpha, theta waves. Gamma waves relate to simultaneous processing of information from different brain areas, as also modulate perception and consciousness. Beta waves are present in our normal waking state of consciousness like when we are engaged to problem solving, decision making etc. Alpha waves dominate in quietly flowing thoughts, calmness and resting state of the brain. During learning, memory, intuition and information beyond our normal state of conscious awareness but also during fears we noticed the theta waves. We decided not to explore the delta waves because they are generated in deepest sleep and meditation, some actions that does not keep up with the research we are conducting.

An 13×13 adjacency matrix was computed that denotes the relation between the ROIs as both sources and destinations. This matrix constructed a graph that we see below with the ROIs as nodes and the calculated connectivity between them as edges. We conduct a statistical analysis on the connectivity matrices in the different datasets. We found that in the period 520 ms untill 10 ms before the 2nd button press there is a statistical significant difference in the measures of the FDI groups. In the visualization procedure, we decided to focus on this period on the Gamma band (30-50 Hz). We examine the Connectivity Magnitude and the Outflow of each ROI. The period we investigated was between 190 ms until 10 ms before the Perceptual Reversal ("second button press"). We added also the period of 110 ms after the reversal between the two groups.

In the picture below we plot the nodes as a function (color and size) of the measure 'Outflow' and the edges as a function (color and size) of 'Connectivity magnitude' at the time point 0.19 sec before the second button press that denotes the perceptual reversal. The 'Outflow' is remarkable on the Right Posterior Cingulate Cortex having the value ≈0.14, when the other ROIs having values less than 0.10. The connectivity (dDTF) between Right Posterior Cingulate Cortex and Caudal Anterior Cingulate constitute a significant connection (≈0.04) comparing with all the others (≈0.01).

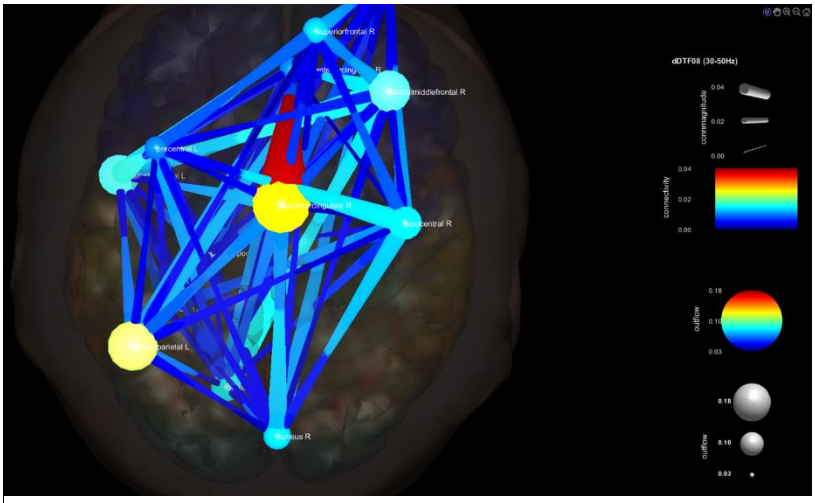

FIGURE 12 A GRAPH CONSTRUCTED FROM THE ADJACENCY MATRIX

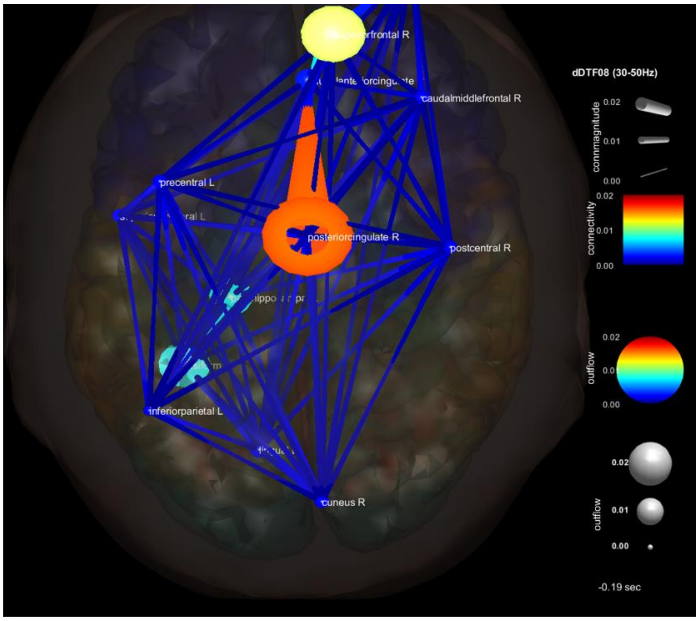
dDTF08 (30-50Hz)
caudalmiddlefrontal R
precentral L
posteriorcingulate R
postcentral R
inferiorparietal L
cuneus R
commagnitude
connectivity
outflow
outflow
-0.19 sec

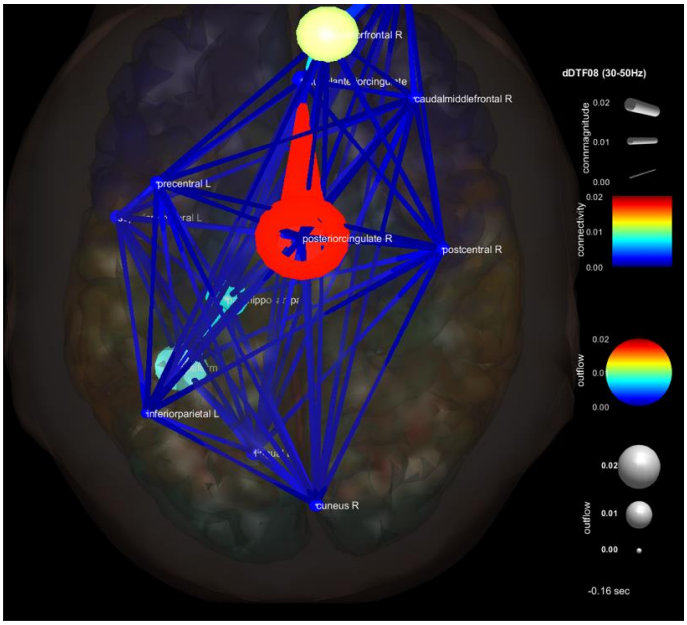
dDTF08 (30-50Hz)
caudalmiddlefrontal R
precentral L
posteriorcingulate R
postcentral R
inferiorparietal L
cuneus R
commagnitude
connectivity
outflow
outflow
-0.16 sec

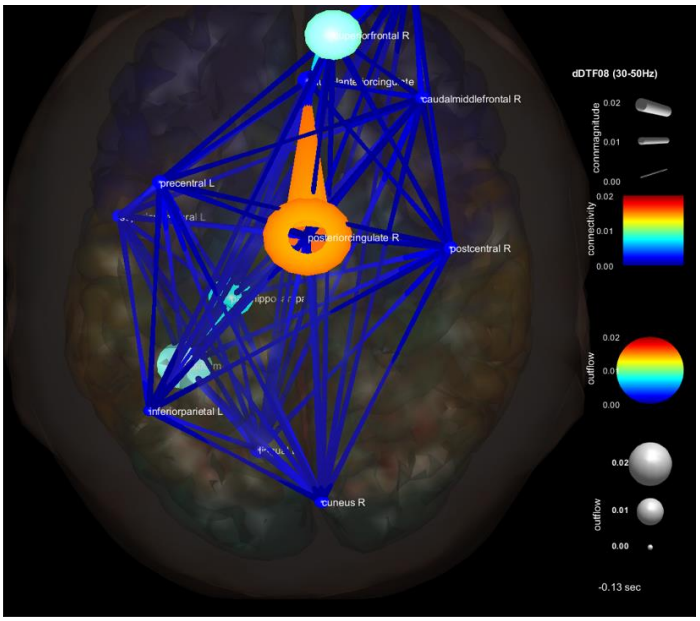
dDTF08 (30-50Hz)
caudalmiddlefrontal R
precentral L
postcentral R
inferiorparietal L
cuneus R
commagnitude
connectivity
outflow
outflow
-0.13 sec

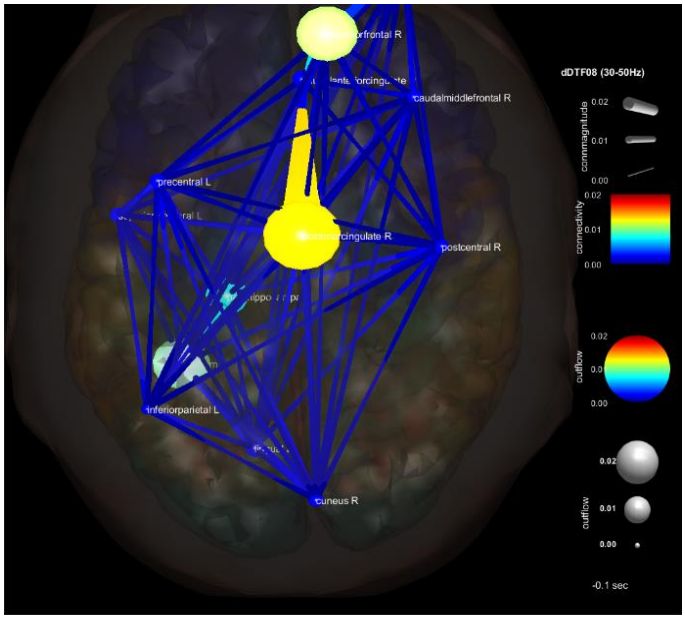
dDTF08 (30-50Hz)
caudalmiddlefrontal R
precentral L
postcentral R
inferiorparietal L
cuneus R
commagnitude
connectivity
outflow
outflow
-0.1 sec

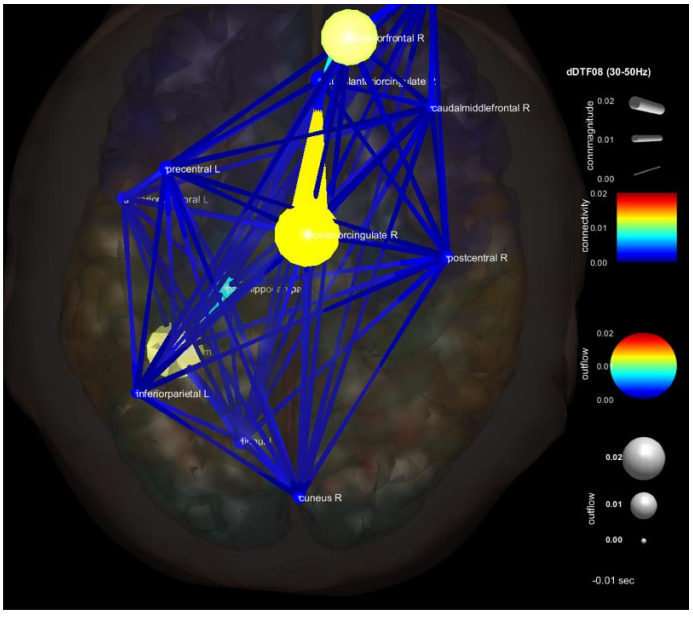
dDTF08 (30-50Hz)
caudalmiddlefrontal R
precentral L
postcentral R
inferiorparietal L
cuneus R
commagnitude
connectivity
outflow
outflow
-0.01 sec

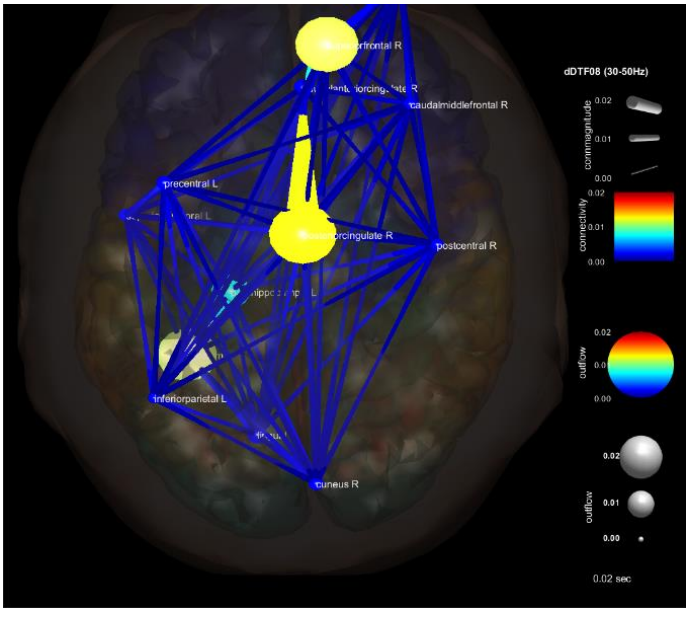
dDTF08 (30-50Hz)
caudalmiddlefrontal R
precentral L
postcentral R
inferiorparietal L
cuneus R
commagnitude
connectivity
outflow
outflow
0.02 sec

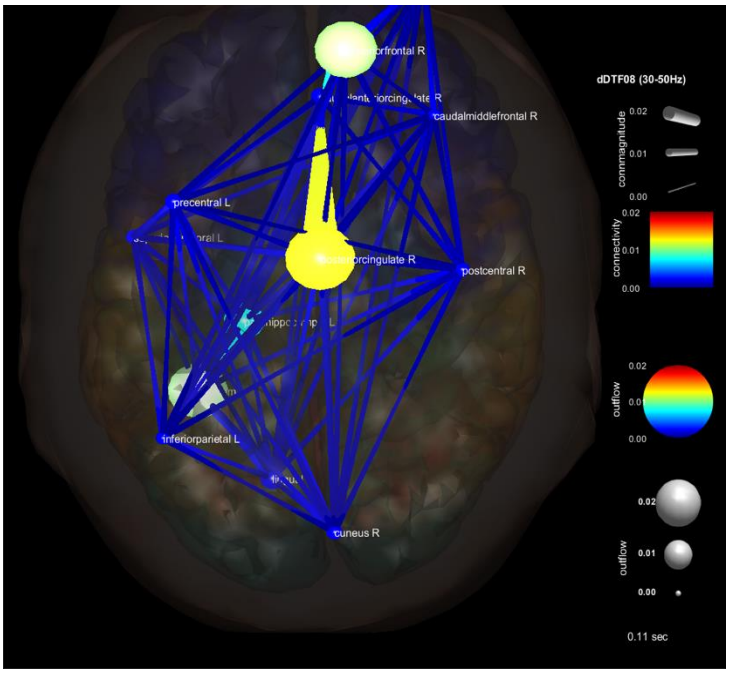

FIGURE 13 FD SUBJECT - GRAPH WITH OUT-STRENGTH VALUES

Comparing the graphs of the two groups we noticed an interesting difference on the value 'Out-strength' or 'Outflow' (SIFT toolbox). In the FD group we noticed in 64.28% of the subjects (9 from 14 subjects) a great 'Outflow' of the Right Posterior Cingulate (PCC) (Outflow≈0.02 and Connectivity Magnitude≈0.02) and Right Superior Frontal (Outflow=0.012) compared to the other ROIs (≈0.007) on the 190 msec before the second button press (perceptual reversal). After this time point, the Right PCC connectivity reduced to 0.015 until 100 ms after the button press. It is important to refer that L fusiform showed a significant activation (Outflow≈0.01) too between 190 ms before the button press until 20 ms after that. Above we see the graph from a FD subject in different time points displaying the 'Outflow' value and below we see the 'Outflow' values across all the brain ROIs in the 0.190 to 0.160 s period.

Field Dependent (Subj. 20)	
	0.190-0.160 s
1. R caudal anterior cingulate	0.0033
2. R caudal middle frontal	0.0014
3. R cuneus	0.0014
4. L fusiform	0.0101
5. L inferior parietal	0.0007
6. L lingual	0.0021
7. L Para hippocampal	0.0079
8. R postcentral	0.0011
9. R posterior cingulate	0.0197
10. L precentral	0.0013
11. R rostral middle frontal	0.0026
12. R superior frontal	0.0128
13. L superior temporal	0.0014

In the pictures below, we noticed an interesting interaction between the Left Para-Hippocampal region and the Left Fusiform in a big percentage of the FI group (71.42%, 5 from 7 subjects). For example, in the FI-Subj 28 the 'Outflow' value of the Para-hippocampal (denoted with red color in the image) is about 0.011 between 190 ms and 160 ms before the second button press. At the same period, Left fusiform's value is less than Para-hippocampal value (denoting with yellow color) but showing a significant value comparing with all the other nodes (≤0.005). This correlation with Para-hippocampal is also visible around 10 ms before the button press.

Field Independent (Subj. 28)	
	0.190-0.160 s
1. R caudal anterior cingulate	0.00055
2. R caudal middle frontal	0.00155
3. R cuneus	0.00055
4. L fusiform	0.00745
5. L inferior parietal	0.00055
6. L lingual	0.00215
7. L Para hippocampal	0.01135
8. R postcentral	0.005
9. R posterior cingulate	0.00225
10. L precentral	0.0005
11. R rostral middle frontal	0.0013
12. R superior frontal	0.0013
13. L superior temporal	0.00105

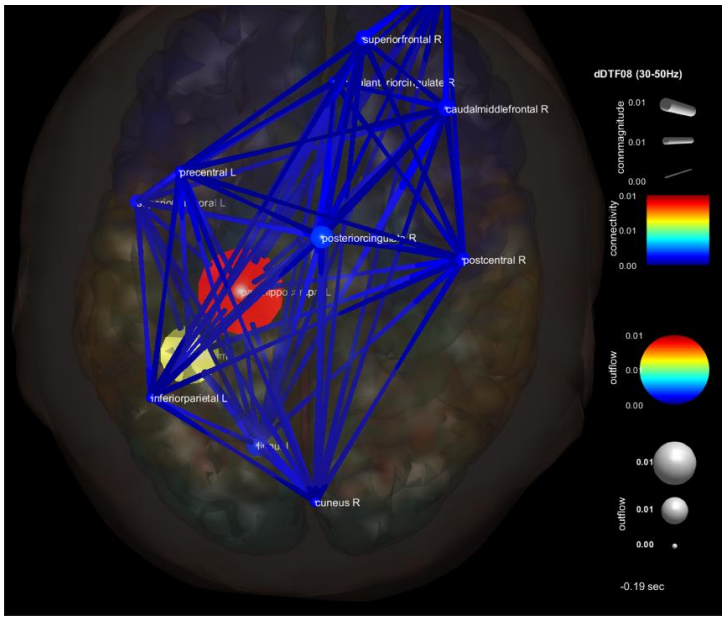

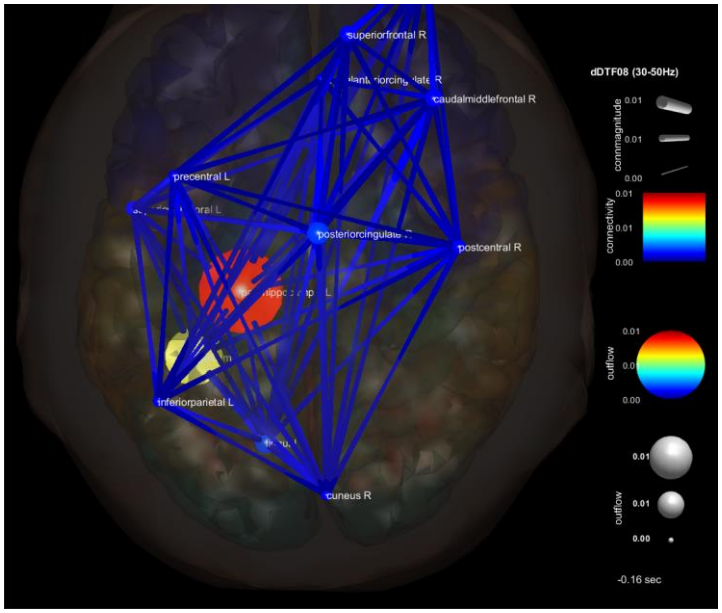

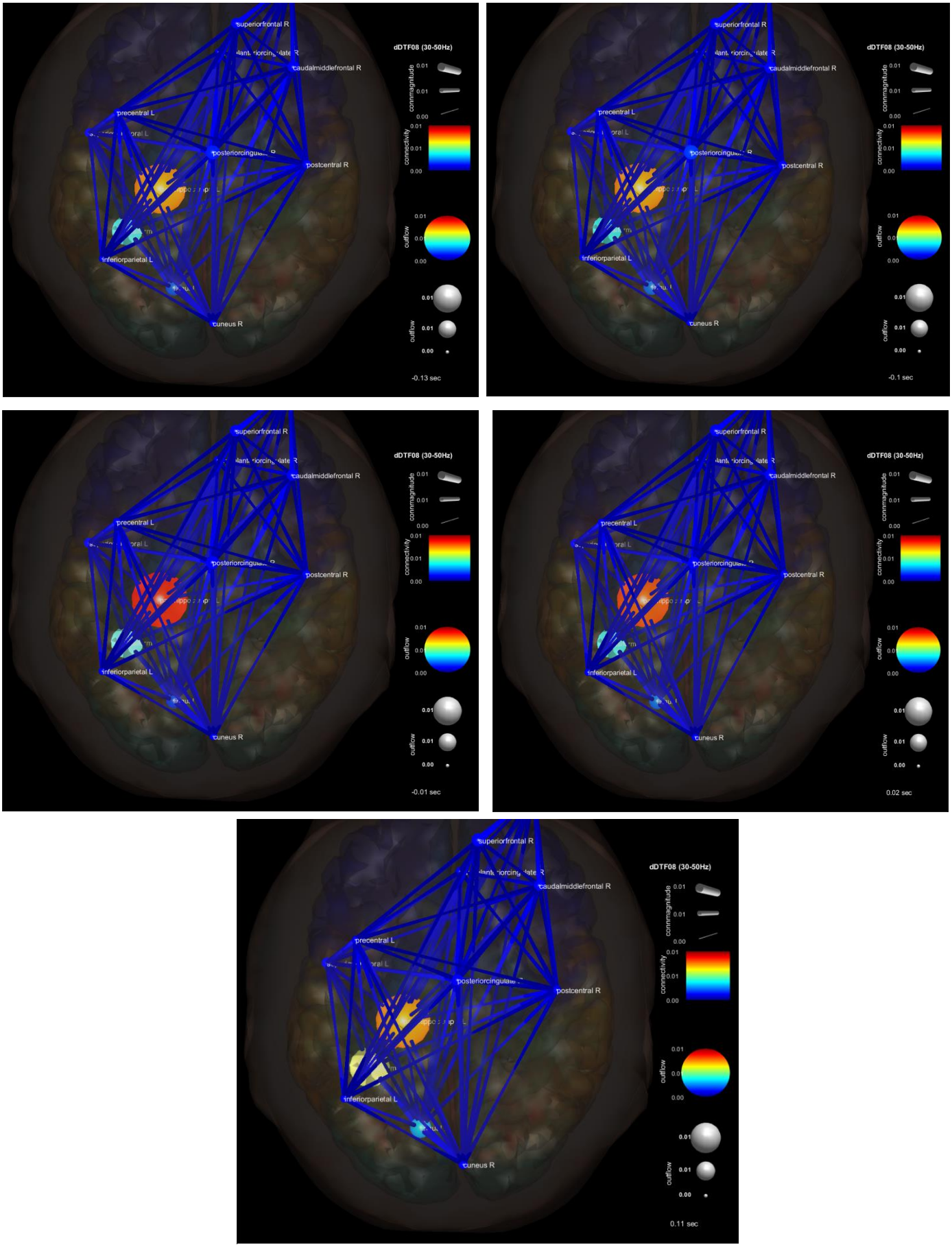

FIGURE 14 FI SUBJECT – GRAPH WITH OUT-STRENGTH VALUES IN DIFFERENT TIME POINTS

From the adjacency matrix, we estimate some basic measures of the graph theory: centrality, strength, in-strength, out-strength, average path length. These metrics allow a characterization of the participants' brain graphs and a further comparison between the two groups, FD and FI. However, without the statistical analysis it will be difficult to see the significance of the differences between them.

6.2 Statistical Results

To interpret the difference between the groups we conducted a statistical analysis procedure. We tested through the D'Agostino-Pearson's K2 test (for assessing normality of data using skewness and kurtosis) if the connectivity values follow the normal distribution. As the connectivity values did not pass the test, we used the non-parametric Mann Whitney test to calculate the statistical significance of our results. The statistical significance of each comparison was evaluated independently by applying the Bonferroni-Holm correction method for solving the multiple comparisons problem (Holm, 1979).

Trial Start

We compare the connectivity features (centrality, characteristic path length, strength, in-strength, out-strength) between Field Dependent and Field Independent participants. Below we see the results from the time period between 100-200 ms after the Trial Start (appearance of the ambiguous image). As we can see there is no statistical significance between the two groups, FD and FI, in any frequency band.

Gamma band (30-50 Hz)	
	p-values
Centrality	**0.2529**
Char Path	**1**
Strength	**0.9018**
In-strength	**0.9368**
Out-strength	**0.9018**

Beta band (13-30 Hz)	
	p-values
Centrality	0.3725
Char Path	0.9671
Strength	0.9671
In-strength	0.8741
Out-strength	0.9671

Alpha Band (8-13 Hz)	
	p-values
Centrality	0.7108
Char Path	0.7108
Strength	0.6504
In-strength	0.8741
Out-strength	0.6504

Theta Band (4-8 Hz)	
	p-values
Centrality	0.2697
Char Path	0.3402
Strength	0.6504
In-strength	0.8741
Out-strength	0.6504

1nd button press (-0.520 s, -0.280 s)

We conducted analysis in the time period 520-280 ms before the first button press that indicates that the subject understands the first figure in an ambiguous image. Still, in this time point there is no statistical significance in the difference of the graph measures between the Field Dependent and Field Independent group except the gamma frequency band. There is no difference in the brain connectivity between the groups during that period of time before the first button press.

Gamma band (30-50 Hz)	
	p-values
Centrality	**0.2220**
Char Path	**1**
Strength	**0.0127***
In-strength	**0.0505**
Out-strength	**0.0621***

Beta band (13-30 Hz)	
	p-values
Centrality	**0.5321**
Char Path	**0.2220**
Strength	**1**
In-strength	**0.7897**
Out-strength	**1**

Alpha Band (8-13 Hz)	
	p-values
Centrality	**0.222**
Char Path	**1**
Strength	**1**
In-strength	**0.7897**

Out-strength	**1**

Theta Band (8-13 Hz)	
	p-values
Centrality	**0.222**
Char Path	**0.222**
Strength	**0.222**
In-strength	**0.1550**
Out-strength	**0.222**

2nd button press (-1 s, 0)

The figures below show that there is a statistical significance in the difference between the groups, 1 sec before the 2nd button press. In between this time period there is a perceptual reversal of the image, specifically the understanding of the second figure in the ambiguous image.

Gamma band (30-50 Hz)		
	p-values	**Bonferroni-Holm correction**
Centrality	**0.1627**	
Char Path	**0.0051***	**0.0102***
Strength	**0.0025***	**0.0100***
In-strength	**0.0091***	**0.0102***
Out-strength	**0.0025***	**0.0100***

Beta band (13-30 Hz)		
	p-values	**Bonferroni-Holm correction**

Centrality	**0.0731**	
Char Path	**0.0153***	**0.0612**
Strength	**0.0153***	**0.0612**
In-strength	**0.0409***	**0.0409***
Out-strength	**0.0153***	**0.0459***

Alpha band (8-13 Hz)		
	p-values	**Bonferroni-Holm correction**
Centrality	**0.2323**	
Char Path	**0.0153***	**0.0153***
Strength	**0.0020***	**0.0080***
In-strength	**0.0074***	**0.0148***
Out-strength	**0.0020***	**0.0080***

Theta band (4-8 Hz)		
	p-values	**Bonferroni-Holm correction**
Centrality	**0.4115**	
Char Path	**0.0153***	**0.0224***
Strength	**0.0032***	**0.0128***
In-strength	**0.0112***	**0.0224***
Out-strength	**0.0032***	**0.0128***

2nd button press (-0.520 s, -0.280 s)

We compare the connectivity features (centrality, characteristic path length, strength, in-strength, out-strength) between Field Dependent and Field Independent participants. We examine now with more accuracy the period before the second button press. The figures below show the mean values of the measures for each group and after the statistical significance of their difference. There is a statistical significance between the

groups, during (-0.520, -0.280) sec before the 2nd button press (the perceptual reversal, the understanding of the second figure in the ambiguous image).

	Gamma band (30-50 Hz)			
	FD	**FI**	**p-values**	**Bonferroni-Holm correction**
Centrality	**16.7033**	**15.0659**	**0.1004**	
Char Path	**9.2164**	**9.6259**	**0.0124***	**0.0124***
Strength	**0.1274**	**0.1233**	**0.0025***	**0.0025***
In-strength	**0.1350**	**0.0616**	**0.0091***	**0.0091***
Out-strength	**0.1447**	**0.0616**	**0.0025***	**0.0025***

	Beta band (13-30 Hz)			
	FD	**FI**	**p-values**	**Bonferroni-Holm correction**
Centrality	**15.9396**	**16.1978**	**0.6815**	
Char Path	**8.5893**	**9.2001**	**0.0153***	**0.0224***
Strength	**0.1499**	**0.1342**	**0.0032***	**0.0128***
In-strength	**0.0699**	**0.0671**	**0.0112***	**0.0224***
Out-strength	**0.0749**	**0.0671**	**0.0032***	**0.0128***

	Alpha band (8-13 Hz)			
	FD	**FI**	**p-values**	**Bonferroni-Holm correction**
Centrality	**16.6374**	**16.3407**	**0.7652**	
Char Path	**7.8882**	**8.4226**	**0.0402***	**0.0402***
Strength	**0.2648**	**0.2369**	**0.0032***	**0.0128***
In-strength	**0.1236**	**0.1185**	**0.0112***	**0.0224***
Out-strength	**0.1324**	**0.1185**	**0.0032***	**0.0128***

	Theta band (4-8 Hz)			
	FD	FI	p-values	Bonferroni-Holm correction
Centrality	16.6264	15.9011	0.1787	
Char Path	7.8675	8.3856	0.0480*	0.0480*
Strength	0.2894	0.2593	0.0051*	0.0204*
In-strength	0.1350	0.1296	0.0165*	0.0330*
Out-strength	0.1447	0.1296	0.0051*	0.0204*

2nd button press (-0.250 s, 0.010 s)

	Gamma band (30-50 Hz)			
	FD	FI	p-values	Bonferroni-Holm correction
Centrality	15.3681	15.7033	0.9109	
Char Path	8.8901	9.6505	0.0032*	0.0064*
Strength	0.1369	0.1231	0.0020*	0.0080*
In-strength	0.0684	0.0616	0.0074*	0.0074*
Out-strength	0.0684	0.0616	0.0020*	0.0080*

	Beta band (13-30 Hz)			
	FD	FI	p-values	Bonferroni-Holm correction
Centrality	15.9725	16.5714	0.8813	
Char Path	8.5773	9.1787	0.0188*	0.0564
Strength	0.1497	0.1493	0.0335*	0.0670
In-strength	0.0698	0.0746	0.0780	
Out-strength	0.0748	0.0746	0.0335*	0.0670

	Alpha band (8-13 Hz)			
	FD	FI	p-values	Bonferroni-Holm correction
Centrality	16.3956	16.1429	0.3905	
Char Path	7.8837	8.5127	0.0081*	0.0162*
Strength	0.2641	0.2369	0.0032*	0.0128*
In-strength	0.1233	0.1184	0.0112*	0.0162*
Out-strength	0.1321	0.1184	0.0032	0.0128

	Theta band (4-8 Hz)			
	FD	FI	p-values	Bonferroni-Holm correction
Centrality	16.2143	16.0659	0.4552	
Char Path	7.9546	8.5057	0.0277*	0.0831
Strength	0.2771	0.2593	0.0277*	0.0831
In-strength	0.1293	0.1296	0.0668	
Out-strength	0.1385	0.1296	0.0277*	0.0554

7. Discussion

We aim to focus on visual ambiguity in FDI groups through a different experimental scheme. Randomly, bistable and normal images lead the subjects to a reversal or a stability trial depending if the perceptual reversal takes place or not. In this study, we use 50 different ambiguous images that lead to reversal or stability trials depending on the subject's ability to recognize the ambiguity or not. Another 50 different unambiguous images are used in our experiment for the control condition. The participants observed the ambiguous and the unambiguous images in a random queue during the task.

There are two experimental schemes used in the ambiguity tasks: the onset paradigm and the manual response paradigm. In our study we used both indicators for calculating the connectivity features. We called the onset of the trial 'Trial Start' point and the subject's manual response 'First Button' point (indicator for distinguishing the first figure of an ambiguous image) and 'Second Button' point (perceptual reversal).

We investigated three periods: one after the 'Trial Start', one before the 'First Button' and a third one before the 'Second Button'. We considered a multivariate autoregressive modeling based analysis consisting of calculation of graph theory connectivity features: betweenness centrality, strength, in-strength, out-strength, average path length. A statistical significance has been noticed between the two FDI groups during the time interval from 520 ms before the 'Second Button' until the 'Second Button' press in the gamma, beta, alpha, and theta band. The fact that during the same period before the 'First button' press we did not notice any statistical significance between the connectivity features of the two groups, declares that there is an essential difference in the brain connectivity on the way they process the perceptual information of the second figure of an ambiguous image between the FDI groups. According to bibliography, a reversal positivity as a P300-like component is occurring about 250 ms before a key press indicating the perceptual reversal (Isoglu-Alkaç et al., 2000; Strüber & Herrmann, 2002). Therefore, our finding confirms that indeed there is a perceptual reversal taking place but closer to 200 ms (perhaps between 190 to 160 ms according with the out-strength values). The statistically significant difference indicates that different brain areas get involved in the perceptual reversal on each FD-I group.

In related publications, the reversal positivity appears around 100 ms after the stimulus onset (Britz et al., 2009; Kornmeier & Bach, 2005, 2006). We calculated the same graph theory connectivity features for the specific time (100 ms after the 'Trial Start'). We concluded that there was no statistically significant difference of the brain connectivity between the two groups while they are watching the ambiguous image for the first time. This finding is maybe explained in the following way. The experimental scheme from the previous studies presents the same ambiguous image in every trial. In contrast, our experiment shows randomized ambiguous images. This fact prevents the participant from having the intention of the specific ambiguity. Because of the randomized order, participants cannot predict the ambiguity of the bistable image. We prove wrong the second theory explaining the reversal phenomenon of ambiguous figures focusing on the intention and learning (Chapter 2, 'the subjects know that a figure is ambiguous and also know that the two perceptions of the image lead them to engage in some form of motivated mental activity pressing for reversal' (Rock et al., 1994)).

Investigating precisely the graph measures, we connect them with the physical meaning they have in human brain. Node betweeness centrality measures how many of the shortest paths between all other node pairs in the network pass through a specific node and captures the relative importance of each node in the brain. A node with high centrality is crucial to efficient communication and as a result a graph with high mean centrality constitutes a graph with important nodes that deleting only one of them could bring effects of perturbations on local or global network states (Bullmore & Sporns, 2009; Freeman, 1977). In our brain graphs, the betweenness centrality measure has not a statistical significant p-value showing that there is no significant difference between the FDI groups on the level of the importance of each node for the graph. The brain regions of the two groups have approximately the same interconnections with their neighbor regions, a fact that makes them equally important for the network. This applies in all the frequency bands we examined.

The mean node strength is the average sum of weights of links connected to the nodes of each graph. In our analysis, we found statistical significance between the FDI groups in the time period 520-10 ms before the 'Second Button' press. This fact could be explained as

different information flow and density of the links in the brain areas evolved in the perceptual reversal between the groups.

The average shortest path length shows statistically significant p-values that exhibit different interconnectedness between the groups. This quantity measures the direct association existing between the brain areas and consequently the brain integrative process. Integration process is the tendency of the brain to synchronize different but relevant areas aiming to early response to stimuli. The FI values of shortest path length were much greater than the FD group respective values during the 520 ms period before the 'Second Button' press in all frequency bands. We propose that the brain integrative process is slightly altered between the groups. The FI group needs more direct node connections in order to perform the same visual perception task. The FD group does not have many direct brain connections between regions and as a result, there is some delay on perceiving the ambiguous image. They have a crux not to transform with nimbleness and velocity their viewpoint in the 3D space of the ambiguous image. Based on a previous study (E. A. Nisiforou, 2015) the FD group makes many saccades for scanning the image, so it seems reasonable that they perceive with some delay and difficulty the second figure at the bistable image and as a consequence having less direct brain connections.

In the level of the brain graphs visualization, in a big percentage (69.23 %) of the FD group, we noticed a significant information outflow in the Right Posterior Cingulate cortex (PCC) compared to the other nodes in the perceptual reversal before the second button press (160-190 ms). The PCC shows strong connectivity to frontal and parietal regions involved in cognitive control (Leech & Sharp, 2014) and engaged in the top-down control of visual attention and eye movements. More specifically, PCC shows a complex pattern of interaction with the fronto-parietal control network (FPCN) and the dorsal attention network in tasks related with visual perception and executive motor control. Also, there are findings that PCC is activated in neuroimaging studies in motivation related tasks showing that may constitute an important site for the integration of motivational and spatial attention information (Engelmann, Damaraju, Padmala, & Pessoa, 2009). As a result, we considered the PCC area as a neural interface between visual attention and different actions (i.e. motor control, motivational decisions), a fact that is strengthened even more by our findings.

In 71.42% of the FI group, we find an interesting interaction between the Left Para-hippocampal and the Fusiform brain area before the second button press (160-190 ms). Para-hippocampal area plays an important role in the encoding and recognition of environmental scenes (as landscapes, cityscapes, or rooms). The fusiform is a structure that is involved in high-level vision; the ability to identify the objects in view based on visual input. However, the connectivity values were not much greater than the values in other brain areas and perhaps it is not necessary to analyze it further (See Table, Chapter 6.1).

Apart from studying each measure independently, we will try to quantify their interaction. We noticed a difference in the brain graph topology between the two groups regarding the direct connections, the density and the weights of the links but there was not a brain area that contributed more than others. The involvement of the brain areas was approximately equally distributed holistically during the task. Despite that, there are alterations in the integration of the brain function in specific time points during the visual perception task indicating that indeed the two groups use different regions for processing of extracting a cue from a complex figure as reported in the Tables of Chapter 6.1. The FD group presents a brain circuit that includes the Right Posterior Cingulate Cortex, an area that is

confirmed that takes part as a main link in tasks that include and executive motor control from previous studies. The FI group shows activation between the Para-hippocampal and Fusiform area in the Left-brain hemisphere.

8. Bibliography

Ariza, E. N. (2002). *Fundamentals of teaching English to speakers of other languages in K-12 mainstream classrooms*. Kendall Hunt.

Başar-Eroglu, C., Strüber, D., Kruse, P., Başar, E., & Stadler, M. (1996). Frontal gamma-band enhancement during multistable visual perception. *International Journal of Psychophysiology*. https://doi.org/10.1016/S0167-8760(96)00055-4

Bell, A. J., & Sejnowski, T. J. (1995). An information-maximization approach to blind separation and blind deconvolution. *Neural Computation*. https://doi.org/10.1162/neco.1995.7.6.1129

Boring, E. G. (1930). A New Ambiguous Figure. *The American Journal of Psychology*. https://doi.org/10.2307/1415447

Britz, J., Landis, T., & Michel, C. M. (2009). Right parietal brain activity precedes perceptual alternation of bistable stimuli. *Cerebral Cortex*. https://doi.org/10.1093/cercor/bhn056

Brockwell, P. J., Dahlhaus, R., & Trindade, A. A. (2005). Modified Burg algorithms for multivariate subset autoregression. *Statistica Sinica*.

Bullmore, E., & Sporns, O. (2009). Complex brain networks: Graph theoretical analysis of structural and functional systems. *Nature Reviews Neuroscience*. https://doi.org/10.1038/nrn2575

Colby, C. L. (2001). *Perception of Extrapersonal Space: Psychological and Neural Aspects*.

Colombo, M. (2013). *Olaf Sporns: Networks of the Brain*. Springer.

Courellis, H., Mullen, T., Poizner, H., Cauwenberghs, G., & Iversen, J. R. (2017). EEG-based quantification of cortical current density and dynamic causal connectivity generalized across subjects performing BCI-monitored cognitive tasks. *Frontiers in Neuroscience*. https://doi.org/10.3389/fnins.2017.00180

Delorme, A., & Makeig, S. (2004). EEGLAB: An open source toolbox for analysis of single-trial EEG dynamics including independent component analysis. *Journal of Neuroscience Methods*. https://doi.org/10.1016/j.jneumeth.2003.10.009

Delorme, A., Mullen, T., Kothe, C., Akalin Acar, Z., Bigdely-Shamlo, N., Vankov, A., & Makeig, S. (2011a). EEGLAB, SIFT, NFT, BCILAB, and ERICA: New tools for advanced EEG processing. *Computational Intelligence and Neuroscience*. https://doi.org/10.1155/2011/130714

Delorme, A., Mullen, T., Kothe, C., Akalin Acar, Z., Bigdely-Shamlo, N., Vankov, A., & Makeig, S. (2011b). EEGLAB, SIFT, NFT, BCILAB, and ERICA: New Tools for Advanced EEG Processing. *Computational Intelligence and Neuroscience*.

https://doi.org/10.1155/2011/130714

Dillon, A., & Watson, C. (1996). User analysis in HCI - The historical lessons from individual differences research. *International Journal of Human Computer Studies*. https://doi.org/10.1006/ijhc.1996.0071

Ding, M., Bressler, S. L., Yang, W., & Liang, H. (2000). Short-window spectral analysis of cortical event-related potentials by adaptive multivariate autoregressive modeling: Data preprocessing, model validation, and variability assessment. *Biological Cybernetics*. https://doi.org/10.1007/s004229900137

Ehrman, M., & Leaver, B. Lou. (2003). Cognitive styles in the service of language learning. *System*. https://doi.org/10.1016/S0346-251X(03)00050-2

Ekstrom, A. D. (2010). Navigation in virtual space: Psychological and neural aspects. *Encyclopedia of Behavioral Neuroscience*, *2*, 286–293.

Ekstrom, R. B., French, J. W., Harman, H. H., & Dermen, D. (1976). *Manual for Kit of Factor-Referenced Cognitive Tests*. (August).

Engelmann, J. B., Damaraju, E., Padmala, S., & Pessoa, L. (2009). Combined effects of attention and motivation on visual task performance: Transient and sustained motivational effects. *Frontiers in Human Neuroscience*. https://doi.org/10.3389/neuro.09.004.2009

Erla, S., Faes, L., Tranquillini, E., Orrico, D., & Nollo, G. (2009). Multivariate Autoregressive Model with Instantaneous Effects to Improve Brain Connectivity Estimation. *Int. J. Bioelectromagn.*

Farmaki, C., Sakkalis, V., Loesche, F., & Nisiforou, E. (2019). Assessing field dependence-independence cognitive abilities through EEG-based bistable perception processing. *Frontiers in Human Neuroscience*, *13*, 345.

Fornito, A., Zalesky, A., & Bullmore, E. T. (2016). Fundamentals of Brain Network Analysis. In *Fundamentals of Brain Network Analysis*. https://doi.org/10.1016/C2012-0-06036-X

Freeman, L. C. (1977). A Set of Measures of Centrality Based on Betweenness. *Sociometry*. https://doi.org/10.2307/3033543

Geweke, J. (1982). Measurement of Linear Dependence and Feedback Between Multiple Time Series. *Journal of the American Statistical Association*. https://doi.org/10.2307/2287238

Goode, P. E., Goddard, P. H., & Pascual-Leone, J. (2002). Event-related potentials index cognitive style differences during a serial-order recall task. *International Journal of Psychophysiology*. https://doi.org/10.1016/S0167-8760(01)00158-1

Gramfort Alexandre, Papadopoulo Théodore, Olivi Emmanuel, & Clerc Maureen. (2010). OpenMEEG: opensource software for quasistatic bioelectromagnetics. *BioMedical Engineering OnLine*. https://doi.org/10.1186/1475-925X-8-1

Granger, C. W. J. (1969). Investigating Causal Relations by Econometric Models and Cross-spectral Methods. *Econometrica*. https://doi.org/10.2307/1912791

Holm, S. (1979). A simple sequentially rejective multiple test procedure. *Scandinavian Journal of Statistics*.

Holmes, C. J., Hoge, R., Collins, L., Woods, R., Toga, A. W., & Evans, A. C. (1998).

Enhancement of MR images using registration for signal averaging. *Journal of Computer Assisted Tomography*. https://doi.org/10.1097/00004728-199803000-00032

Honey, C. J., Kötter, R., Breakspear, M., & Sporns, O. (2007). Network structure of cerebral cortex shapes functional connectivity on multiple time scales. *Proceedings of the National Academy of Sciences of the United States of America*. https://doi.org/10.1073/pnas.0701519104

Hytti, H., Takalo, R., & Ihalainen, H. (2006). Tutorial on multivariate autoregressive modelling. *Journal of Clinical Monitoring and Computing*. https://doi.org/10.1007/s10877-006-9013-4

Intaite, M., Koivisto, M., Rukšenas, O., & Revonsuo, A. (2010). Reversal negativity and bistable stimuli: Attention, awareness, or something else? *Brain and Cognition*. https://doi.org/10.1016/j.bandc.2010.06.002

Isoglu-Alkaç, Ü., Basar-Eroglu, C., Ademoglu, A., Demiralp, T., Miener, M., & Stadler, M. (2000). Alpha activity decreases during the perception of Necker cube reversals: An application of wavelet transform. *Biological Cybernetics*. https://doi.org/10.1007/s004220050585

Kamiński, M., Ding, M., Truccolo, W. A., & Bressler, S. L. (2001). Evaluating causal relations in neural systems: Granger causality, directed transfer function and statistical assessment of significance. *Biological Cybernetics*. https://doi.org/10.1007/s004220000235

Kaminski, M. J., & Blinowska, K. J. (1991). A new method of the description of the information flow in the brain structures. *Biological Cybernetics*. https://doi.org/10.1007/BF00198091

Kannathal, N., Choo, M. L., Acharya, U. R., & Sadasivan, P. K. (2005). Entropies for detection of epilepsy in EEG. *Computer Methods and Programs in Biomedicine*. https://doi.org/10.1016/j.cmpb.2005.06.012

Karl, J. F. (1994). Functional and effective connectivity in neuroimaging: A synthesis. *Human Brain Mapping*. https://doi.org/10.1002/hbm.460020107

Kemp, B., & Olivan, J. (2003). European data format "plus" (EDF+), an EDF alike standard format for the exchange of physiological data. *Clinical Neurophysiology*. https://doi.org/10.1016/S1388-2457(03)00123-8

Kitajo, K., Hanakawa, T., Ilmoniemi, R. J., & Miniussi, C. (2015). *Manipulative approaches to human brain dynamics*. Frontiers Media SA.

Korhonen, I., Mainardi, L., Loula, P., Carrault, G., Baselli, G., & Bianchi, A. (1996). Linear multivariate models for physiological signal analysis: Theory. *Computer Methods and Programs in Biomedicine*. https://doi.org/10.1016/0169-2607(96)01764-6

Kornmeier, J., & Bach, M. (2005). The Necker cube - An ambiguous figure disambiguated in early visual processing. *Vision Research*. https://doi.org/10.1016/j.visres.2004.10.006

Kornmeier, J., & Bach, M. (2006). Bistable perception - along the processing chain from ambiguous visual input to a stable percept. *International Journal of Psychophysiology*. https://doi.org/10.1016/j.ijpsycho.2006.04.007

Kornmeier, J., & Bach, M. (2012). Ambiguous figures - what happens in the brain when perception changes but not the stimulus. *Frontiers in Human Neuroscience*. https://doi.org/10.3389/fnhum.2012.00051

Kornmeier, J., & Bach, M. (2014). EEG correlates of perceptual reversals in Boring's ambiguous old/young woman stimulus. *Perception*. https://doi.org/10.1068/p7741

Korzeniewska, A., Crainiceanu, C. M., Kuś, R., Franaszczuk, P. J., & Crone, N. E. (2008). Dynamics of event-related causality in brain electrical activity. *Human Brain Mapping*. https://doi.org/10.1002/hbm.20458

Korzeniewska, A., Mańczak, M., Kamiński, M., Blinowska, K. J., & Kasicki, S. (2003). Determination of information flow direction among brain structures by a modified directed transfer function (dDTF) method. *Journal of Neuroscience Methods*. https://doi.org/10.1016/S0165-0270(03)00052-9

Kuś, R., Kamiński, M., & Blinowska, K. J. (2004). Determination of EEG activity propagation: Pair-wise versus multichannel estimate. *IEEE Transactions on Biomedical Engineering*. https://doi.org/10.1109/TBME.2004.827929

Lachaux, J. P., Lutz, A., Rudrauf, D., Cosmelli, D., Le Van Quyen, M., Martinerie, J., & Varela, F. (2002). Estimating the time-course of coherence between single-trial brain signals: An introduction to wavelet coherence. *Neurophysiologie Clinique*. https://doi.org/10.1016/S0987-7053(02)00301-5

Lancaster, J. L., Woldorff, M. G., Parsons, L. M., Liotti, M., Freitas, C. S., Rainey, L., … Fox, P. T. (2000). Automated Talairach Atlas labels for functional brain mapping. *Human Brain Mapping*. https://doi.org/10.1002/1097-0193(200007)10:3<120::AID-HBM30>3.0.CO;2-8

Lee, D. S., Kye, W. H., Rim, S., Kwon, T. Y., & Kim, C. M. (2003). Generalized phase synchronization in unidirectionally coupled chaotic oscillators. *Physical Review E - Statistical Physics, Plasmas, Fluids, and Related Interdisciplinary Topics*. https://doi.org/10.1103/PhysRevE.67.045201

Lee, L., Harrison, L. M., & Mechelli, A. (2003). The Functional Brain Connectivity Workshop: Report and commentary. *Network: Computation in Neural Systems*. https://doi.org/10.1088/0954-898X/14/2/201

Leech, R., & Sharp, D. J. (2014). The role of the posterior cingulate cortex in cognition and disease. *Brain*. https://doi.org/10.1093/brain/awt162

Litvak, V., Mattout, J., Kiebel, S., Phillips, C., Henson, R., Kilner, J., … Friston, K. (2011). EEG and MEG data analysis in SPM8. *Computational Intelligence and Neuroscience*. https://doi.org/10.1155/2011/852961

Lütkepohl, H. (2005). New introduction to multiple time series analysis. In *New introduction to Multiple Time Series Analysis*. https://doi.org/10.1007/978-3-540-27752-1

Lütkepohl, H. (2006). Structural vector autoregressive analysis for cointegrated variables. In *Modern Econometric Analysis: Surveys on Recent Developments*. https://doi.org/10.1007/3-540-32693-6_6

Makeig, S. (1993). Auditory event-related dynamics of the EEG spectrum and effects of exposure to tones. *Electroencephalography and Clinical Neurophysiology*. https://doi.org/10.1016/0013-4694(93)90110-H

Makeig, S., Debener, S., Onton, J., & Delorme, A. (2004). Mining event-related brain dynamics. *Trends in Cognitive Sciences*. https://doi.org/10.1016/j.tics.2004.03.008

Maksimenko, V. A., Frolov, N. S., Hramov, A. E., RUNNOVA, A. E., Grubov, V. V, Kurths, J., &

Pisarchik, A. N. (2019). Neural Interactions in a Spatially-Distributed Cortical Network During Perceptual Decision-Making. *Frontiers in Behavioral Neuroscience*, *13*, 220.

Mathes, B., Strüber, D., Stadler, M. A., & Basar-Eroglu, C. (2006). Voluntary control of Necker cube reversals modulates the EEG delta- and gamma-band response. *Neuroscience Letters*. https://doi.org/10.1016/j.neulet.2006.03.063

Matousek, M. (1973). *Frequency and Correlation Analysis. Handbook of Electroencephalography and Clinical Neurophysiology. Vol. 5, Part A*. Amsterdam: Elsevier.

Miron, E., Erez, M., & Naveh, E. (2004). Do personal characteristics and cultural values that promote innovation, quality, and efficiency compete or complement each other? *Journal of Organizational Behavior*. https://doi.org/10.1002/job.237

Mullen, T. R. (2014). The Dynamic Brain: Modeling Neural Dynamics and Interactions From Human Electrophysiological Recordings. *ProQuest Dissertations and Theses*.

Naraghipour, H., & Baghestani, A. (n.d.). *The Difference between Field-Dependent versus Field-Independent EFL Learners' Use of Learning Strategies*.

Nash-Kille, A., & Sharma, A. (2014). Inter-trial coherence as a marker of cortical phase synchrony in children with sensorineural hearing loss and auditory neuropathy spectrum disorder fitted with hearing aids and cochlear implants. *Clinical Neurophysiology*. https://doi.org/10.1016/j.clinph.2013.11.017

Nisiforou, E. A. (2015). Examining the association between users creative thinking and field dependence-independence cognitive style through eye movement components. *C and C 2015 - Proceedings of the 2015 ACM SIGCHI Conference on Creativity and Cognition*. https://doi.org/10.1145/2757226.2764556

Nisiforou, E. A., & Laghos, A. (2013). Do the eyes have it? Using eye tracking to assess students cognitive dimensions. *Educational Media International*. https://doi.org/10.1080/09523987.2013.862363

Nisiforou, E., & Laghos, A. (2016). Field Dependence-Independence and Eye Movement Patterns: Investigating Users' Differences Through an Eye Tracking Study. *Interacting with Computers*. https://doi.org/10.1093/iwc/iwv015

Node Degree and Strength. (2016). In *Fundamentals of Brain Network Analysis*. https://doi.org/10.1016/b978-0-12-407908-3.00004-2

Ojeda, A., Klug, M., Kreutz-Delgado, K., Gramann, K., & Mishra, J. (2019). *A Bayesian framework for unifying data cleaning, source separation and imaging of electroencephalographic signals*. https://doi.org/10.1101/559450

Palva, J. M., Palva, S., & Kaila, K. (2005). Phase synchrony among neuronal oscillations in the human cortex. *Journal of Neuroscience*. https://doi.org/10.1523/JNEUROSCI.4250-04.2005

Parkkonen, L., Andersson, J., Hämäläinen, M., & Hari, R. (2008). Early visual brain areas reflect the percept of an ambiguous scene. *Proceedings of the National Academy of Sciences of the United States of America*. https://doi.org/10.1073/pnas.0810966105

Pereda, E., Quiroga, R. Q., & Bhattacharya, J. (2005). Nonlinear multivariate analysis of neurophysiological signals. *Progress in Neurobiology*. https://doi.org/10.1016/j.pneurobio.2005.10.003

Pion-Tonachini, L., Kreutz-Delgado, K., & Makeig, S. (2019). ICLabel: An automated electroencephalographic independent component classifier, dataset, and website. *NeuroImage*. https://doi.org/10.1016/j.neuroimage.2019.05.026

Renard, Y., Lotte, F., Gibert, G., Congedo, M., Maby, E., Delannoy, V., … Lécuyer, A. (2010). OpenViBE: An open-source software platform to design, test, and use brain-computer interfaces in real and virtual environments. *Presence: Teleoperators and Virtual Environments*. https://doi.org/10.1162/pres.19.1.35

Rock, I., Hall, S., & Davis, J. (1994). Why do ambiguous figures reverse? *Acta Psychologica*. https://doi.org/10.1016/0001-6918(94)90065-5

Sakkalis, V. (2011). Review of advanced techniques for the estimation of brain connectivity measured with EEG/MEG. *Computers in Biology and Medicine*. https://doi.org/10.1016/j.compbiomed.2011.06.020

Sakkalis, Vangelis. (2011). Applied strategies towards EEG/MEG biomarker identification in clinical and cognitive research. *Biomarkers in Medicine*. https://doi.org/10.2217/bmm.10.121

Sakkalis, Vangelis, Tsiaras, V., & Tollis, I. G. (2010). Graph analysis and visualization for brain function characterization using EEG data. *Journal of Healthcare Engineering*. https://doi.org/10.1260/2040-2295.1.3.435

Schlögl, A. (2006a). A comparison of multivariate autoregressive estimators. *Signal Processing*. https://doi.org/10.1016/j.sigpro.2005.11.007

Schlögl, A. (2006b). *GDF - A general dataformat for biosignals*. 1–16. Retrieved from http://arxiv.org/abs/cs/0608052

Schlögl, A., & Supp, G. (2006). Chapter 9 Analyzing event-related EEG data with multivariate autoregressive parameters. *Progress in Brain Research*. https://doi.org/10.1016/S0079-6123(06)59009-0

Schreiber, T. (2000). Measuring information transfer. *Physical Review Letters*. https://doi.org/10.1103/PhysRevLett.85.461

Strüber, D., & Herrmann, C. S. (2002). MEG alpha activity decrease reflects destabilization of multistable percepts. *Cognitive Brain Research*. https://doi.org/10.1016/S0926-6410(02)00139-8

Tass, P., Rosenblum, M. G., Weule, J., Kurths, J., Pikovsky, A., Volkmann, J., … Freund, H. J. (1998). Detection of n:m phase locking from noisy data: Application to magnetoencephalography. *Physical Review Letters*. https://doi.org/10.1103/PhysRevLett.81.3291

Tononi, G., Sporns, O., & Edelman, G. M. (1994). A measure for brain complexity: Relating functional segregation and integration in the nervous system. *Proceedings of the National Academy of Sciences of the United States of America*. https://doi.org/10.1073/pnas.91.11.5033

Wang, M., Arteaga, D., & He, B. J. (2013). Brain mechanisms for simple perception and bistable perception. *Proceedings of the National Academy of Sciences of the United States of America*. https://doi.org/10.1073/pnas.1221945110

Wang, X., Sang, N., Hao, L., Zhang, Y., Bi, T., & Qiu, J. (2017). Category selectivity of human visual cortex in perception of Rubin Face-Vase illusion. *Frontiers in Psychology*.

https://doi.org/10.3389/fpsyg.2017.01543

Weilnhammer, V., Stuke, H., Hesselmann, G., Sterzer, P., & Schmack, K. (2017). A predictive coding account of bistable perception - a model-based fMRI study. *PLoS Computational Biology*. https://doi.org/10.1371/journal.pcbi.1005536

Wen, Q., & Chklovskii, D. B. (2005). Segregation of the Brain into Gray and White Matter: A Design Minimizing Conduction Delays. *PLoS Computational Biology*. https://doi.org/10.1371/journal.pcbi.0010078

Zhang, L. (2004). Field-dependence/independence: cognitive style or perceptual ability?—validating against thinking styles and academic achievement. *Personality and Individual Differences*, *37*(6), 1295–1311.

Acknowledgement

I would like to thank my thesis supervisor Vangelis Sakkalis for his help and support conducting this research. I would also like to thank Adonis Moschovakis and Stelios Smyrnakis for the help and the excellent cooperation we had. In addition, I would like to recognize the contribution that Christina Farmaki provided during my study. I would like to acknowledge Giorgos Christodoulakis, Iraklis Skepasianos, Manos Koutoulakis, Maira Tampakaki and Marilena Oraiopoulou for helping me solving various technical problems in this research and for their unlimited support.

A special thanks to my friends Elisavet Stamoulou and Margarita Malliou for supporting me for everything even in the hard times. I would also like to thank my dear Master classmates Violetta Manola, Ira Kostopoulou, Gianna Potsi, Mourat Vezir, Angeliki Gleni, Michalis, Eleni Skourti, Giorgos G. and Alexandros for their passionate encouragement. I wish to acknowledge the Cretan Climbing Community, my brothers and sisters, for helping me stay mentally and naturally healthy.

I must express my gratitude to my mother Efi, my father Yiannis, my siblings Maria, Stella and Lymperis for providing me with unfailing support and continuous encouragement through my years of study and through this research. I would like to thank also my grandmother Maria and Kaiti and my grandfather Stelios for their love.